HELICOPTER DYNAMICS

Inderjit Chopra
Anubhav Datta

ENAE 633 Helicopter Dynamics
Spring 2011

Contents

1 Introduction to Rotor Dynamics **9**
1.1 Basic Rotor Aerodynamics 9
1.1.1 Hover 9
1.1.2 Axial Climb 23
1.1.3 Axial Descent 25
1.1.4 Forward Flight 26
1.2 Basic Structural Dynamics 32
1.2.1 Second-Order Systems 32
1.2.2 Reduction to First-Order Form 39
1.2.3 Rotor Blade Dynamics 41
1.2.4 Flap motion of a rotor blade 42
1.3 Aero-elastic Response 45
1.3.1 Flap response for non-rotating blades 46
1.3.2 Flap response for rotating blades in vacuum 46
1.3.3 Flap response in hover 47
1.3.4 Flap response in forward flight 48
1.4 Introduction to Loads 52
1.4.1 Root shear load 53
1.4.2 Root bending load 53
1.4.3 Rotating frame hub loads 53
1.4.4 Fixed frame hub loads 54
1.5 Rotor planes of reference 57
1.6 Helicopter Trim 61
1.6.1 Rotor Forces and Moments 62
1.6.2 Uncoupled trim 64
1.6.3 Coupled trim for an isolated rotor 65
1.6.4 Coupled trim for a full aircraft 66
1.6.5 Rotor Power and Lift to Drag Ratio 71
1.6.6 The Jacobian Method for Trim 76

2 Flap Dynamics **79**
2.1 Rigid Blade Model 79
2.1.1 Hinged Blade with zero offset 79
2.1.2 Hinged Blade with Offset 82
2.1.3 Hingeless Blade with Equivalent Hinge Offset 85
2.2 Flexible Beam Model 86
2.2.1 Axial Deformation 86
2.2.2 Euler-Bernoulli Theory of Bending 86
2.2.3 Flap Bending Equation using Newtons's Laws 87
2.2.4 Second Order Nonlinear Coupled Axial Elongation-Flap Bending 90

2.2.5 Axial Elongation as a Quasi-coordinate . . . 94
2.2.6 Boundary Conditions . . . 94
2.3 Non-rotating beam vibration . . . 95
2.3.1 Cantilevered Beam . . . 96
2.3.2 Simple-Supported Beam . . . 99
2.3.3 Beam Functions . . . 99
2.4 Rotating Beam Vibration . . . 100
2.4.1 Approximate solution Methods . . . 101
2.4.2 Galerkin Method . . . 101
2.4.3 Rayleigh-Ritz Method . . . 105
2.5 Finite Element Method (FEM) . . . 111
2.5.1 Element properties . . . 112
2.5.2 Assembly of elements . . . 114
2.5.3 Constraint conditions . . . 117
2.6 Fan plot and frequency plots for rotating beams . . . 119
2.6.1 Rotating versus non-rotating frequencies . . . 119
2.6.2 Rotating frequencies vs. rotational speed . . . 119
2.6.3 Rotating versus non-rotating mode shapes . . . 127
2.7 Response Solution in time . . . 129
2.7.1 Fourier series methods . . . 130
2.7.2 Finite Element in Time (FET) method . . . 133
2.7.3 Time Integration Methods . . . 136
2.8 Bending Moments and Stresses . . . 136
2.8.1 Deflection and Force Summation methods . . . 136
2.8.2 Force summation vs. modal method . . . 138
2.9 Fourier Coordinate Transformation . . . 138
2.9.1 FCT of governing equations . . . 140
2.10 Aeroelastic Stability . . . 145
2.10.1 Stability roots in hover . . . 146
2.11 Stability Analysis in Forward flight . . . 151
2.11.1 Constant Coefficient System . . . 151
2.11.2 Periodic coefficient systems . . . 153
2.11.3 Floquet stability solution . . . 153
2.11.4 Floquet response solution . . . 154

3 Coupled Flap-Lag-Torsion Dynamics **163**
3.1 Lag Dynamics . . . 163
3.1.1 Rigid Lag Model with Hinge Offset . . . 163
3.1.2 Elastic Lag Model . . . 165
3.1.3 Natural Vibrations of Lag Motion . . . 167
3.1.4 Finite Element Formulation . . . 169
3.2 Torsion Dynamics . . . 171
3.2.1 Rigid Torsion Model . . . 172
3.2.2 Elastic Torsion . . . 175
3.2.3 Natural Vibrations of Torsion Motion . . . 177
3.2.4 Beam Functions for Torsion . . . 177
3.3 Coupled Flap-Lag Dynamics . . . 178
3.3.1 Rigid Model . . . 178
3.3.2 Flexible Model . . . 183
3.4 Coupled Pitch-Flap Dynamics . . . 185

3.4.1 Rigid Model . . . 185
3.4.2 Kinematic Pitch-Flap Coupling: δ_3 Effect . . . 188
3.4.3 δ_3 Effect in Hover . . . 189
3.4.4 Kinematic Pitch-Lag Coupling: δ_4 Effect . . . 191
3.5 Rigid Flap-Lag-Torsion . . . 192
3.6 Flexible Flap-Lag-Torsion-extension . . . 196
3.6.1 Second order non-linear beam model . . . 196
3.6.2 Equations for uniform beams . . . 196
3.6.3 Detailed model for non-uniform beams . . . 197
3.6.4 Blade Coordinate Systems . . . 197
3.6.5 Blade Deformation Geometry . . . 198
3.6.6 Nondimensionalization and Ordering scheme . . . 202
3.6.7 Formulation Using Hamilton's Principle . . . 203
3.6.8 Derivation of Strain Energy . . . 204
3.6.9 Derivation of Kinetic Energy . . . 207
3.6.10 Virtual Work . . . 210
3.6.11 Equations of Motion . . . 210
3.7 Structural loads . . . 211
3.7.1 Modal Curvature Method . . . 212
3.7.2 Force Summation Method . . . 212
3.8 Hub Reactions . . . 214

4 Unsteady Aerodynamics 221
4.1 Basic Fluid Mechanics Equations . . . 221
4.1.1 Navier-Stokes equations . . . 222
4.1.2 Euler equations . . . 226
4.1.3 Velocity Potential Equation for Unsteady Flows . . . 226
4.1.4 The Acceleration Potential . . . 229
4.1.5 Vorticity Conservation Equation . . . 230
4.1.6 Potential Equation for Steady Flow . . . 231
4.1.7 Potential Equation for Incompressible Flow . . . 231
4.2 The Rotor Flow Field . . . 232
4.2.1 Wake Structure of a Lifting Wing . . . 232
4.2.2 Coupled Airloads and Wake . . . 233
4.2.3 Non-steady Excitation in Rotor Blades . . . 234
4.2.4 Trailed and Shed Wake Structure of a Rotor . . . 234
4.2.5 Unsteady Aerodynamics . . . 235
4.2.6 Dynamic Stall . . . 235
4.3 Unsteady Thin Airfoil Theory . . . 237
4.3.1 Steady Airloads . . . 239
4.3.2 Quasi-Steady Airloads . . . 240
4.3.3 Unsteady Airloads . . . 242
4.3.4 A Simple Interpretation . . . 246
4.3.5 The Theodorsen Lift Deficiency Function . . . 247
4.3.6 Application to Rotary Wings . . . 248
4.3.7 Near Shed Wake . . . 251
4.3.8 Time-Varying Free Stream . . . 252
4.3.9 Returning Wake . . . 252
4.3.10 Miller's Conclusion . . . 254
4.4 Time Domain Methods for Unsteady Aerodynamics . . . 254

4.4.1 Leishman-Beddoes indicial model 257
4.4.2 Frequency response of indicial model 258
4.4.3 Recursive formulation of an indicial model 263
4.4.4 Leishman-Beddoes dynamic stall formulation 265
4.5 Wing Models 269
4.5.1 Prandtl Lifting Line Theory 269
4.5.2 Weissinger-L Lifting-surface Theory 270
4.5.3 Unsteady Lifting-Line Analysis 272
4.6 Perturbation Aerodynamic Forces 274
4.7 Dynamic Inflow Models 280
4.7.1 Hover 280
4.7.2 Forward Flight 280

5 Aeroelastic Stability in Hover 287
5.1 Flag-Lag Flutter 287
5.1.1 Comment on Flap-Lag Flutter 295
5.2 Pitch-Flap Instabilities 300
5.2.1 Pitch Divergence 302
5.2.2 Flutter 304
5.3 Flap-Lag-Torsion Flutter 307

6 Ground and Air Resonance 319
6.1 Ground Resonance 319
6.1.1 Blade Lag Motion in Fixed Coordinates 319
6.1.2 Three and Four bladed Rotors 320
6.1.3 Ground Resonance Equations 322
6.2 Ground Resonance of Two-Bladed Rotors 330
6.3 Air Resonance 333
6.3.1 Body Pitch and Roll with a Rigid Spinning Rotor 335
6.3.2 Rotor Flap and Lag 335
6.3.3 Rotor Flap and Body Pitch 339
6.3.4 Rotor Flap and Body Pitch and Roll 339
6.3.5 Rotor Flap and Lag and Body Pitch in Vacuum 340
6.3.6 Rotor Flap and Lag coupled to Body Pitch and Roll in Air 344
6.4 Experimental Data on Aeromechanical Stability 347

7 Aeroelastic Stability in Forward Flight 363
7.1 Flap Motion in forward flight 363
7.2 Hover Stability Roots 365
7.3 Forward Flight Stability Roots 366
7.3.1 Stability Roots in Rotating Coordinates 367
7.3.2 Stability Roots in Fixed Coordinates 367
7.4 Flap-lag Stability in Forward Flight 369
7.4.1 Perturbation Stability Solution 371
7.4.2 Constant Coefficient Approximation 373
7.4.3 Floquet Theory 373

8 Trailing Edge Flaps and Tabs **377**
8.1 Flap-Torsion-Aileron Dynamics of a Wing Section . . . 377
8.1.1 Flap-Torsion dynamics . . . 377
8.1.2 Flap-torsion-Aileron dynamics: Force method . . . 378
8.1.3 Flap-torsion-Aileron dynamics: Energy method . . . 379
8.2 Flap-Torsion-Aileron-Tab Dynamics of a Rotor Blade . . . 380
8.2.1 Governing equations . . . 380
8.2.2 Hinge Moments . . . 391
8.2.3 Initial condition response . . . 391
8.2.4 Response with prescribed tab deflections . . . 391
8.2.5 Flap-Torsion-Aileron Dynamics for a Rotor Blade . . . 392
8.2.6 Response using prescribed aileron deflections . . . 393
8.2.7 Flap-Torsion-Aileron-Tab equations in non-dimensional form . . . 393
8.3 Aerodynamic Model . . . 395
8.3.1 Theodorsen model for aileron . . . 395
8.3.2 Theodorsen and Garrick model for aileron and tab . . . 396
8.3.3 2D airfoil data . . . 402
8.4 Flexible blade equations . . . 405

9 CFD for Rotors **415**
9.1 Isentropic Flow Relations . . . 415
9.1.1 Unsteady Bernoulli's Equation . . . 417
9.1.2 Pressure coefficient . . . 418
9.2 Potential equation in the non-conservation form . . . 418
9.2.1 Blade fixed moving frame . . . 419
9.2.2 Velocity and acceleration in the moving frame . . . 420
9.2.3 Derivatives in the moving frame . . . 421
9.2.4 Full Potential Equations . . . 422
9.2.5 Boundary conditions . . . 424
9.2.6 Small disturbance equations for subsonic and transonic flows . . . 425
9.2.7 Literature . . . 427
9.3 Potential equation in conservation form . . . 427
9.3.1 Full potential equation . . . 428
9.3.2 Generalized coordinate transformation . . . 428
9.3.3 Literature . . . 430
9.4 Euler and Navier-Stokes equations . . . 430
9.4.1 Review of Curvilinear coordinates . . . 430
9.4.2 Generalized coordinate transformation . . . 433
9.4.3 Euler equation in generalized coordinates . . . 434
9.4.4 Thomas and Lombard's Geometric Conservation Law . . . 438
9.4.5 Navier-Stokes equations in generalized coordinates . . . 439
9.4.6 Surface Boundary Conditions . . . 441

10 Helicopter Vibration **443**
10.1 Measure of Helicopter Vibration . . . 443
10.2 Sources of Helicopter Vibration . . . 444
10.3 Analysis of Helicopter Vibration . . . 445
10.4 Rotor Vibratory Loads . . . 446
10.4.1 Periodic Blade Forcing . . . 448
10.4.2 Hub Loads in Rotating Frame . . . 449
10.4.3 Hub Loads in Fixed Frame . . . 450

10.5 Vibration Control 452
10.6 Passive Vibration Control 453
10.6.1 Vibration Isolators 453
10.6.2 Vibration Absorbers 454
10.6.3 Bifilar Pendulum absorber 454
10.7 Active Vibration Control 455
10.7.1 Multicyclic Vibration Control or Higher Harmonic Control (HHC) 455
10.7.2 Control Algorithms 457
10.7.3 Off–line Identification 459
10.7.4 On–line Identification 460
10.7.5 Open–Loop Off–Line Control 461
10.7.6 Closed–Loop Off–Line Control 461
10.7.7 Open–Loop On–Line Control 462
10.7.8 Closed–Loop On–Line Control 463

11 Rotor Tests in Wind Tunnel and in Flight **469**
11.1 Wind Tunnel Models 469
11.1.1 Froude-Scaled Models 470
11.1.2 Mach-Scaled Models 472
11.1.3 Model Fabrication 473
11.1.4 Model Instrumentation 473
11.2 Model Testing 474
11.2.1 Testing for Isolated Rotor Stability 475
11.2.2 Spectra for Various Inputs 475
11.3 Major Model and Full Scale Rotor Tests 475

Chapter 1

Introduction to Rotor Dynamics

The objective of this chapter is to introduce the topic of rotor dynamics, as applied to rotorcraft. Helicopters are the most common form of a rotorcraft. It has a single main rotor, and a smaller tail rotor. Some rotorcraft have multiple main rotors like the tandem, co-axial, and tilt-rotor aircraft. Some have unusual configurations like a compound with a wing and propeller, a stopped or slowed rotor, or a quad tilt-rotor with two wings and 4 main rotors. The main rotor, or rotors form the heart of every rotorcraft. To begin the study of rotor dynamics one needs familiarity with the following concepts. The purpose of this chapter is to introduce these concepts.

1) Basic rotor aerodynamics
2) Basic Structural Dynamics
3) Aero-elastic Response
4) Loads
5) Helicopter trim

Typically, a helicopter rotor has a large diameter, and produces thrust at disk loadings (thrust per unit area) of 2-10 lbs/ft^2 (200-450 N/m^2). It consists of two, three, four or sometimes five to seven blades. The blades are like large aspect ratio wings (chord/Radius $\sim$ 15), made of special airfoil sections. The U.S. manufactured blades rotate counter clockwise (looking from above facing toward helicopter). The rotor RPM is generally around 300-400. The tip speeds are of the order of 700 ft/sec. The speed at which it sucks in air, called the downwash velocity, is in comparision around 30-50 ft/sec. There is a small diameter rotor at the far end of the body called the tail rotor. The purpose of the tail rotor is to counterbalance the shaft torque reaction of main rotor and provide directional stability to the vehicle. Let us briefly examine the aerodynamics of two major flight modes of the helicopter, hover and forward flight.

1.1 Basic Rotor Aerodynamics

1.1.1 Hover

Hover is a flight condition of the helicopter with zero forward speed and zero vertical speed. The flow condition on the rotor disk is axisymmetric. Momentum theory is widely used to calculate the minimum power that is necessary to generate a given thrust using a given disk area. First, the velocity with which the surrounding air needs to be sucked in through the rotor to generate the thrust, is calculated. This velocity is also called rotor downwash or inflow. The power is then simply the thrust multiplied with inflow. Larger the rotor diameter, smaller the inflow for a given thrust, and hence smaller the power requirement.

Momentum theory does not tell us whether a rotor will be able to generate a given thrust. The rotor may stall before an intended thrust level is achieved. The blade element theory can be used to calculate the maximum thrust capability. The blade element theory is discussed later.

Momentum Theory

Momentum theory assumes a uniform, incompressible, zero-swirl flow through the rotor disk. It uses the three basic laws of fluid mechanics: conservation of mass, conservation of momentum, and conservation of energy. It solves for the three unknowns: the inflow velocity, v, the velocity of the fully contracted far wake, w, and the fully contracted flow area, A_4. The flow around a rotor in hover is shown in Fig. 1.1 The total pressures at each of the four stations are

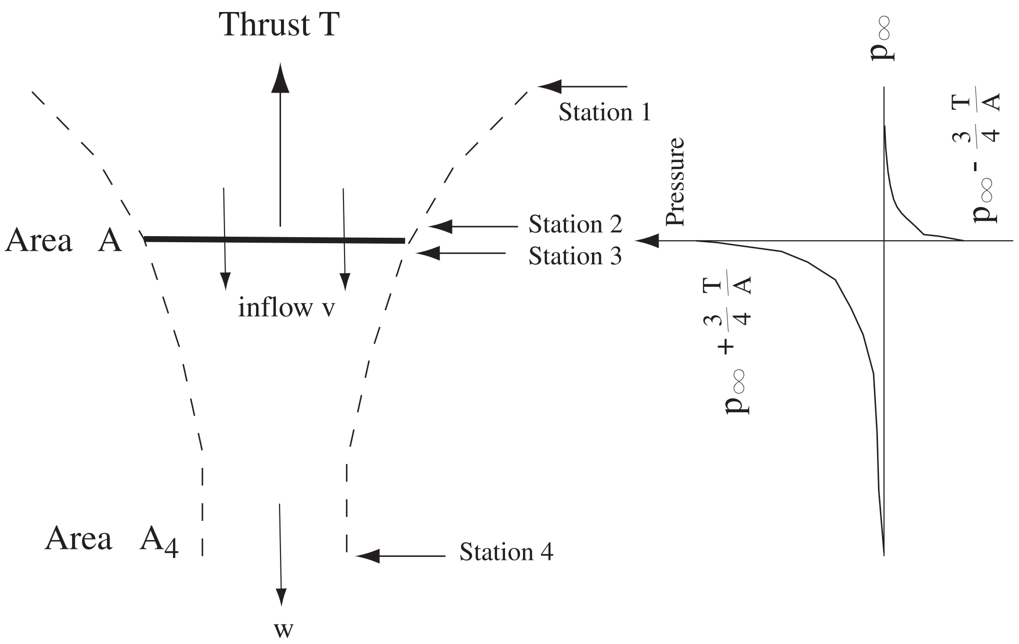

Figure 1.1: **Flow around a rotor in hover**

$$
\begin{aligned}
p_{01} &= p_\infty \quad \text{static pressure far upstream} \\
p_{02} &= p_2 + \tfrac{1}{2}\rho v^2 \\
p_{03} &= p_3 + \tfrac{1}{2}\rho v^2 \\
p_{04} &= p_\infty + \tfrac{1}{2}\rho w^2
\end{aligned}
$$

As no force is applied on the fluid between sections 1 and 2, and then between sections 3 and 4, there is no change in total pressure.

$$
\begin{aligned}
p_{02} &= p_{01} \\
p_{03} &= p_{04}
\end{aligned}
$$

Force is only applied on the fluid between sections 2 and 3, leading to the pressure differential

$$
p_3 - p_2 = \frac{T}{A}
$$

Thus

$$
\begin{aligned}
p_2 &= p_{02} - \tfrac{1}{2}\rho v^2 \\
&= p_\infty - \tfrac{1}{2}\rho v^2 \\
p_3 &= p_{03} - \tfrac{1}{2}\rho v^2 \\
&= p_{04} - \tfrac{1}{2}\rho v^2 \\
&= p_\infty + \tfrac{1}{2}\rho w^2 - \tfrac{1}{2}\rho v^2
\end{aligned}
$$

Therefore

$$p_3 - p_2 = \frac{1}{2}\rho w^2$$

Equating this with the pressure differential we have

$$T = \frac{1}{2}\rho A w^2$$

where A is the disk area. Upto this was conservation of energy. Conservation of momentum gives

$$\begin{aligned} T &= \text{mass flow rate . change in fluid velocity} \\ &= \rho A v(w - 0) \end{aligned}$$

Equating the expressions from conservation of momentum and conservation of energy we have

$$w = 2v$$

Thus the air which is at rest far upstream is accelerated by the rotor to velocity v at the disc, and then to velocity $2v$ far downstream. It follows

$$T = 2\rho A v^2$$

The induced velocity and induced power are then

$$v = \sqrt{\frac{T}{2\rho A}}$$

$$P = \frac{T^{3/2}}{\sqrt{2\rho A}}$$

In addition, from conservation of mass, the far downstream flow area is

$$A_4 = \frac{A}{2}$$

The pressures above and below the rotor disk are given as

$$\begin{aligned} p2 &= p_\infty - \tfrac{1}{2}\rho v^2 \\ &= p_\infty - \tfrac{1}{4}\tfrac{T}{A} \\ p3 &= p_\infty + \tfrac{1}{2}\rho w^2 - \tfrac{1}{2}\rho v^2 \\ &= p_\infty + \tfrac{3}{2}\rho v^2 \\ &= p_\infty + \tfrac{3}{4}\tfrac{T}{A} \end{aligned}$$

The induced velocity v can be non-dimesionalized as

$$\lambda = \frac{v}{\Omega R}$$

where

$$\begin{aligned} \Omega &= \text{rotational speed (rad/sec)} \\ R &= \text{rotor radius (ft)} \end{aligned}$$

The thrust and power can be non-dimensionalized as

$$C_T = \frac{T}{\rho A (\Omega R)^2}$$

$$C_P = \frac{P}{\rho A(\Omega R)^3}$$

Using T $= 2\rho A v^2$ in the above expression produces a relation between inflow ratio λ and the thrust coefficient

$$\lambda = \sqrt{\frac{c_T}{2}}$$

Note that this relation is based on uniform flow through the entire rotor disk. To cover nonuniform flow, tip losses, and momentum loss due to swirl flow, an empirical correction factor κ_h is used

$$\lambda = \kappa_h \sqrt{\frac{c_T}{2}}$$

Typically, $\kappa_h = 1.15$. The power coefficient then becomes

$$C_P = \lambda C_T = \kappa_h \frac{C_T^{3/2}}{\sqrt{2}}$$

The Momentum theory assists in the preliminary evaluation of a rotor and helps in the comparison of various rotors. However, the theory does not help directly with the design of a rotor.

Blade Element Theory

To calculate the aerodynamic force distribution on the blade, the simple blade element theory is widely used. It is also called 2-dimensional (2D) Strip Theory. Each blade element is a 2D airfoil which is assumed to operate independantly of the other elements. The aerodynamic forces acting on each blade element are the lift, drag, and pitching moments. They are called air loads.

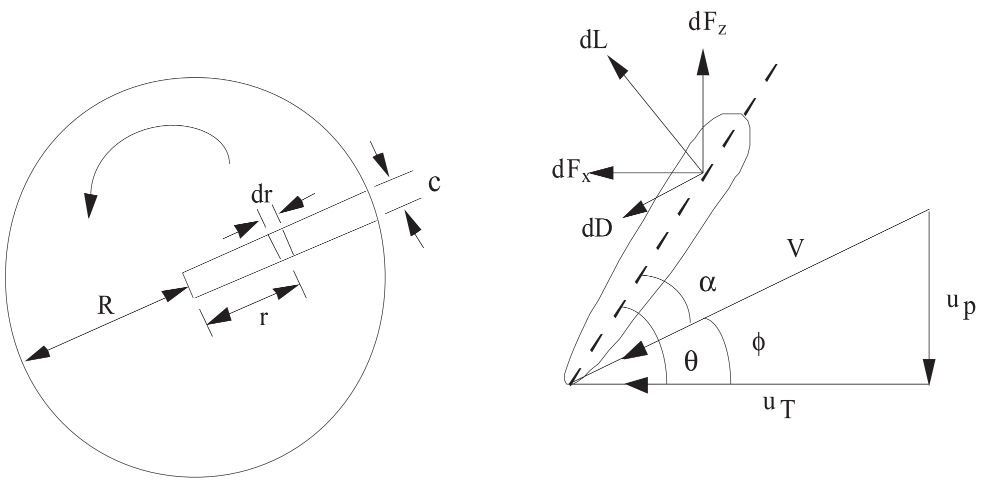

$$\begin{aligned}
U_T &= \text{tangential velocity (in the plane of rotation)} \\
U_P &= \text{normal velocity} \\
V &= \text{resultant velocity} \sqrt{U_P^2 + U_T^2} \\
&\cong U_T^2 \\
\theta &= \text{pitch angle} \\
\alpha &= \text{effective angle of attack} \\
&= \theta - \tan^{-1}\frac{U_P}{U_T} \cong \theta - \frac{U_P}{U_T} \\
dL &= \text{lift generated on an element of length dr located at a radial station r} \\
&= \frac{1}{2}\rho V^2 c_l\, c\, dr \\
c &= \text{chord} \\
c_l &= \text{lift coefficient} \\
&= a\left(\theta - \frac{U_p}{U_T}\right) \\
a &= \text{airfoil lift curve slope (linear below stall)} \\
dD &= \text{element drag force} \\
&= \frac{1}{2}\rho V^2 c_d\, c\, dr
\end{aligned}$$

Resolved force components are

$$\begin{aligned}
dF_z &= dL\,\cos\phi - dD\,\sin\phi \\
&\cong dL \\
&= \frac{1}{2}\rho U_T^2 ca\left(\theta - \frac{U_P}{U_T}\right) dr \\
&= \frac{1}{2}\rho ca\left(\theta U_T^2 - U_P U_T\right) dr \\
dF_x &= dL\,\sin\phi + dD\,\cos\phi \\
&\cong \frac{U_p}{U_T} dL + dD \\
&= \frac{1}{2}\rho ca\left(\theta U_T U_P - U_P^2\right) dr + \frac{1}{2}\rho U_T^2 c c_d dr
\end{aligned}$$

The rotor thrust T, torque Q, and power P are

$$\begin{aligned}
\mathrm{T} &= \text{Total forces from } N_b \text{ blades} \\
&= N_b \int_0^R dF_z \\
\mathrm{Q} &= \text{Total torque from } N_b \text{ blades} \\
&= N_b \int_0^R r dF_x \\
\mathrm{P} &= \Omega \mathrm{Q}
\end{aligned}$$

Assume, for simplicity, an uniform induced inflow on the disk. Later on we will see that this assumption is strictly true only for ideally twisted blades. Before we study ideal twist, and other twist distributions, consider a zero twist case. For a zero twist rotor, the blades have a constant pitch angle, θ across the blade span. We have

$$c_l = a\left(\theta - \frac{U_P}{U_T}\right)$$

For hover

$$\begin{aligned} U_T &= \Omega r \\ U_p &= \lambda \Omega R \end{aligned}$$

Consider the following non-dimensionalizations. First, define a solidity ratio as the ratio of total blade area to disk area. For uniform chord blades

$$\sigma = \frac{N_b c}{\pi R}$$

A local solidity ratio can be defined as

$$\sigma(r) = \frac{N_b c(r)}{\pi R}$$

Also

$$\begin{aligned} x &= \frac{r}{R} \\ u_t &= \frac{U_T}{\Omega R} = x \\ u_p &= \frac{U_P}{\Omega R} = \lambda \end{aligned}$$

Thrust coefficient

$$\begin{aligned} c_T &= \frac{T}{\rho A (\Omega R)^2} \\ &= \frac{N_b \int_0^R \frac{1}{2}\rho c a \left(\theta u_t^2 - u_p u_t\right) dr}{\rho(\pi R^2)} \\ &= \frac{\frac{1}{2} a N_b c \int_0^1 \left(\theta x^2 - \lambda x\right) dx}{\pi R} \\ &= \frac{\sigma a}{2}\int_0^1 \left(\theta x^2 - \lambda x\right) dx \\ &= \frac{\sigma a}{2}\left(\frac{\theta}{3} - \frac{\lambda}{2}\right) \end{aligned}$$

Now consider a linear twist distribution

$$\theta = \theta_{75} + \theta_{tw}\left(\frac{r}{R} - \frac{3}{4}\right)$$

Here θ_{75} is the pitch at 75% radius position and θ_{tw} is the linear twist distribution. Again assuming a uniform induced inflow λ, one obtains

$$\begin{aligned} c_T &= \frac{\sigma a}{2}\int_0^1 \left(\theta_{75} x^2 + \theta_{tw} x^3 - \frac{3}{4}\theta_{tw} x^2 - \lambda x\right) dx \\ &= \frac{\sigma a}{2}\left(\frac{\theta_{75}}{3} - \frac{\lambda}{2}\right) \end{aligned}$$

Note that the twist distribution θ_{tw} has got cancelled. Thus, it is a general relationship valid for both uniform pitch and linearly twisted blades. From momentum theory, induced inflow is

$$\lambda = \kappa_h \sqrt{\frac{c_T}{2}}$$

The thrust level is related to the pitch setting

$$c_T = \frac{\sigma a}{2}\left(\frac{\theta_{75}}{3} - \frac{1}{2}\kappa_h \sqrt{\frac{c_T}{2}}\right)$$

$$\theta_{75} = 6\frac{c_T}{\sigma a} + \frac{3}{2}\kappa_h \sqrt{\frac{c_T}{2}}$$

Thus, blade element theory gives the blade setting required to generate an inflow of $\kappa_h \sqrt{\frac{C_T}{2}}$, which in turn is necessary to produce a particular thrust coefficient C_T. Note that the assumption here is that the airfoils do not stall at angle of attack produced by this pitch setting, and operates at at the lift curve slope a.

Now consider the torque coefficient for a constant pitch setting and uniform chord.

$$\begin{aligned}
\text{Torque } Q &= N_b \int_0^R r\, dF_x \\
&= N_b \int_0^R \frac{1}{2}\rho c a \left(U_P U_T \theta - U_P^2 + U_T^2 \frac{C_{do}}{a}\right) r dr \quad \text{assuming} \quad c_d = c_{do}
\end{aligned}$$

The Torque coefficient is

$$\begin{aligned}
C_Q &= \frac{Q}{\rho(\pi R^2)(\Omega R)^2 R} \\
&= \frac{N_b \frac{1}{2}\rho a c \int_0^R \left[\lambda \Omega R.\Omega r \theta - (\lambda \Omega R)^2 + (\Omega R)^2 \frac{c_{do}}{a}\right] r dr}{\rho(\pi R^2)(\Omega R)^2 R} \\
&= \frac{\sigma a}{2} \int_0^1 \left(\theta \lambda x^2 - \lambda^2 x + \frac{c_{do}}{a} x^3\right) dx \\
&= \lambda \frac{\sigma a}{2} \int_0^1 \left(\theta x^2 - \lambda x\right) dx + \frac{\sigma a}{2} \int_0^1 \frac{c_{do}}{a} x^3 dx \\
&= \lambda C_T + \frac{\sigma a}{2} \int_0^1 \frac{c_{do}}{a} x^3 dx \\
&= \lambda C_T + \frac{\sigma c_{do}}{8}
\end{aligned}$$

For example, using the C_T expression for uniform pitch we can get

$$C_Q = \frac{\sigma a}{2} \lambda \left(\frac{\theta}{3} - \frac{\lambda}{2}\right) + \frac{\sigma}{8} C_{do}$$

Note that C_Q has broken up into two parts, one related to C_T, the other related to sectional drag.

$$C_Q = C_{Qi} + C_{Qo}$$

These are called the induced torque, and profile torque.

The Power coefficient, by definition, is identical to the torque coefficient. Thus the induced power and profile power are identical to induced torque and profile torque.

$$\begin{aligned}
C_P &= \frac{P}{\rho(\pi R^2)(\Omega R)^3} \\
&= \frac{\Omega Q}{\Omega\rho(\pi R^2)(\Omega R)^2 R} \\
&= C_Q \\
&= C_{Pi} + C_{Po}
\end{aligned}$$

The induced power is the power spent to generate thrust. It is an absolute minimum, without which the thrust cannot be sustained. It is spent to push the airflow downwards. In an ideal case the entire induced power would be spent on pushing the airflow downwards. In reality a part of the induced power is lost in swirl flow, tip losses, non-uniform inflow. This can be accounted for, as we saw before, using the factor κ_h. The profile power is spent to overcome drag. We would like this to be minimized as much as possible. An important parameter is used to estimate the hover performance of a rotor. It is called the Figure of Merit, M. The Figure of Merit, M, is defined as the ration of ideal power to the actual power.

$$\begin{aligned}
M &= \frac{(C_{pi})_{\text{ideal}}}{(C_{pi})_{\text{real}} + C_{po}} \\
&= \frac{(\lambda C_T)_{\text{ideal}}}{(\lambda C_T)_{\text{real}} + \frac{\sigma}{8} C_{do}} \\
&= \frac{\frac{C_T^{3/2}}{\sqrt{2}}}{\kappa_h \frac{C_T^{3/2}}{\sqrt{2}} + \frac{\sigma}{8} C_{do}}
\end{aligned}$$

Typically, the value of M lies between 0.6 to 0.8. The higher value is more true for recent rotors. From the above expression it seems that a rotor operating at high C_T would have a high M, other factors remaining constant. Indeed, as C_T increases, M assymptotes to κ_h. In reality it is different. Airfoil stall prevents the other factors from remaining constant. Even though C_T is high, the sectional c_l should still be below stall. The sectional c_l is directly related to rotor $\frac{C_T}{\sigma}$. Thus the solidity, σ, has to be increased as well. Alternatively, the sectional c_l may be pushed up close to stall. In this case the airfoil drag increases. Using simply c_{do} as a constant drag is no longer an acceptable assumption. Thus it is impossible to keep increasing C_T indefinitely without increasing the second factor in the denominator.

Shaft horsepower

$$\text{HP} = \frac{P}{550} \qquad \text{(P ft-lb)}$$

Example 1.1: In a circulation-controlled airfoil, a thin jet of air is blown from a spanwise slot along a rounded trailing edge. Due to the Coanda effect, the jet remains attached by balance of centrifugal force and suction pressure. For a CCR, the thrust can be controlled by geometric pitch as well as blowing.

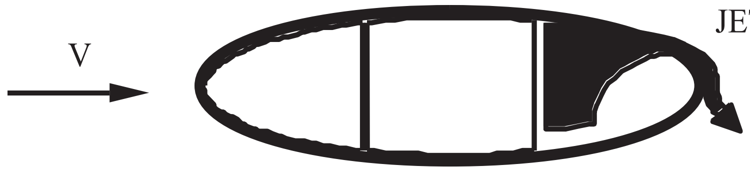

QUASI-ELLIPTIC

Assuming lift coefficient $c_l = c_1\alpha + c_2\mu$, establish a relationship between thrust coefficient, c_T, geometric pitch, θ_o (uniform), and blowing coefficient, c_μ (uniform), for a hovering rotor. Assume a uniform inflow condition.

For hover

$$
\begin{aligned}
U_P &= \lambda\Omega R \\
U_T &= \Omega r \\
T &= N_b \int_0^R dF_z \\
&= N_b \int_0^R \frac{1}{2}\rho c \Omega^2 r^2 c_l dr \\
c_l &= c_1\alpha + c_2\mu \\
&= c_1\left(\theta_0 - \frac{\lambda}{x}\right) + c_2\mu
\end{aligned}
$$

CIRCULATION CONTROL CONCEPT

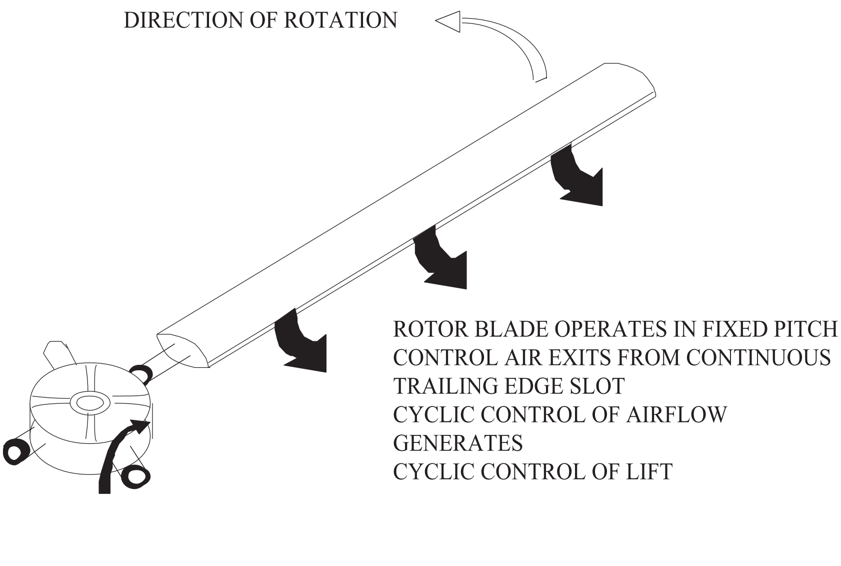

$$\begin{aligned}
c_T &= \frac{T}{\rho\pi R^2(\Omega R)^2} \qquad \text{and} \qquad \sigma = \frac{N_b c}{\pi R} \\
&= \frac{\sigma}{2}\int_0^1 x^2 \left[c_1\left(\theta_0 - \frac{\lambda}{x}\right) + c_2 c_\mu\right] dx \\
&= \frac{\sigma}{2}\left[c_1\left(\frac{\theta_0}{3} - \frac{\lambda}{2}\right) + \frac{1}{3}c_2 c_\mu\right] \\
\lambda &= \kappa_h\sqrt{\frac{c_T}{2}} \\
\theta_0 &= \frac{6c_T}{\sigma c_1} + \frac{3}{2}\lambda + \frac{c_2}{c_1}c_\mu
\end{aligned}$$

Momentum Theory in Annular Form

In the earlier derivations, the induced velocity was assumed to be uniform over the rotor disk. In reality, the inflow is highly non-uniform. The non-uniformity in inflow can be calculated and accounted for by using what is called the Combined Blade Element Momentum Theory. It combines Blade Element Theory with Momentum Theory. The momentum theory is used in its annular form. The idea is simple. The momentum theory is simply applied to an annular ring of thickness, dr, located at radial position, r, extended both far upstream and far downstream. For this elemental ring, the induced velocity in the far wake is again twice the induced velocity at the disk. Thus the thrust on the annular ring

$$\begin{aligned}
dT = &= \text{mass flow rate . change in fluid velocity} \\
&= \rho dAv(w-0) \\
&= \rho(2\pi r dr)v(2v-0) \\
&= 4\rho v^2 \pi r dr \\
dC_T &= 4\lambda^2 x dx
\end{aligned}$$

Combined Blade Element Momentum Theory

Combines momentum theory and blade element theory to obtain non-uniform spanwise induced velocity, or inflow, distribution. From blade element theory we had the following expressions.

$$\begin{aligned}
dC_T &= \frac{N_b\, dF_z}{\rho A(\Omega R)^2} \\
&= \frac{1}{2}\sigma a\left(\theta - \frac{\lambda}{x}\right)x^2 dx \\
&= \frac{1}{2}\sigma c_l(x) x^2 dx
\end{aligned}$$

Earlier when we integrated the above expression to obtain C_T, we assumed $\sigma(x) = \sigma$, a constant for convenience. Here, we leave it in general to be a function of radial station. Thus is it the local solidity.

$$c_l(x) = a(\theta - \frac{\lambda}{x})$$

$$\begin{aligned}
dC_P &= dC_Q \\
&= \frac{N_b\; r\, dF_x}{\rho A(\Omega R)^2 R} \\
&= \frac{1}{2}\sigma\left(c_l\phi + c_d\right)x^3 dx \qquad \text{where} \quad \phi = \frac{\lambda}{x} \\
&= \frac{1}{2}\sigma c_l \phi x^3 dx + \frac{1}{2}\sigma c_d x^3 dx \\
&= dC_{Pi} + dC_{P0}
\end{aligned}$$

Let us obtain an expression for sectional bound circulation. The bound circulation is obtained using 2D Kutta condition. The Kutta condition relates the span-wise gradient of blade lift $\frac{dL}{dr}$ to the bound circulation $\Gamma(r)$ using following the simple relation

$$\frac{dL}{dr} = \rho U \Gamma(r)$$

where U is the local incident flow velocity. Keeping in mind, that the blade lift in hover is simply the rotor thrust divided by the number of blades, it follows

$$\begin{aligned}
dL(r) &= \rho U_T \Gamma(r) dr \\
dT(r) &= N_b \rho U_T \Gamma(r) dr \\
dC_T(r) &= \frac{N_b}{\Omega A} x\Gamma(x)dx \qquad \text{Now use blade element expression on the left} \\
\frac{1}{2}c_l(x)x^2 dx &= \frac{N_b}{\Omega A} x\Gamma(x)dx \qquad \text{From here it follows} \\
\Gamma(x) &= \frac{1}{2}\Omega\frac{\sigma A}{N_b}c_l(x)x \\
&= \frac{1}{2}\Omega c(x)Rc_l(x)x \qquad \text{dimension } m^2/s \\
\gamma(x) &= \frac{\Gamma(x)}{\Omega R} \\
&= \frac{1}{2}\frac{c(x)}{R}c_l(x)x \qquad \text{non-dimensional}
\end{aligned}$$

Now we have all the necessary equations to study the results of Combined Blade Element Momentum Theory. The theory gives us a method to calculate non-uniform inflow across the span. Simply relate the dC_T expressions from Blade Element and Annular Momentum theories.

$$\frac{1}{2}\sigma a\left(\theta - \frac{\lambda}{x}\right)x^2 dx = 4\lambda^2 x dx$$

Solve for λ as a function of x

$$\lambda(x) = \sqrt{A^2 + B\theta x} - A \tag{1.1}$$

where

$$\begin{aligned}
A &= \frac{\sigma a}{16} \\
B &= \frac{\sigma a}{8}
\end{aligned}$$

Another interesting expression can be obtained as follows. Instead of really solving for λ we can re-arrange the above equation to read as

$$\begin{aligned}\frac{1}{2}\sigma(x)c_l x^2 dx &= 4\lambda^2 dx \\ \frac{1}{2}\sigma(x)a\alpha x^2 dx &= 4\lambda^2 dx\end{aligned}$$

which gives

$$\lambda = \sqrt{\frac{\sigma x a\alpha}{8}} \tag{1.2}$$

Note that, the α above is the sectional angle of attack $\theta - \lambda/x$, with a λ hiding inside. Let us now study the effect of different twist distributions. Consider the following cases one by one.

Case I : $\theta = \theta_{75} = \text{const}$

$$\begin{aligned}\lambda(x) &\cong \text{linear} \cong \lambda_0 x \\ c_l(x) &\cong a(\theta_{75} - \lambda_0) = \text{constant} \\ \Gamma(x) &\cong \text{linear} \\ dC_T(x) &\cong \text{parabolic} \\ C_T &= \frac{1}{2}\sigma a\left(\frac{\theta_{75}}{3} - \frac{\lambda}{2}\right)\end{aligned}$$

Case II : $\theta(x) = \theta_0 + x\theta_{tw}$

$$\begin{aligned}\lambda(x) &= \text{non-uniform} \\ c_l(x) &= \text{non-uniform} \\ \Gamma(x) &= \text{non-uniform} \\ dC_T(x) &= \text{non-uniform} \\ C_T &= \frac{1}{2}\sigma a\left(\frac{\theta_0}{3} + \frac{\theta_{tw}}{4} - \frac{\lambda}{2}\right) \\ &= \frac{1}{2}\sigma a\left(\frac{\theta_{75}}{3} - \frac{\lambda}{2}\right)\end{aligned}$$

Case III : $\theta(x) = \frac{\theta_{tip}}{x}$

$$\begin{aligned}\lambda(x) &= \text{const} \\ &= \phi x \\ &= \phi_{tip} \\ c_l(x) &= \frac{1}{x}a(\theta_{tip} - \phi_{tip}) \\ &= \frac{1}{x}\alpha_{tip} \qquad \text{hyperbolic} \\ \Gamma(x) &= \text{const} \\ dC_T(x) &= \text{linear} \\ &= \frac{1}{2}\sigma a\alpha_{tip} x dx \\ C_T &= \frac{1}{4}\sigma a\alpha_{tip} \qquad \text{assume constant } \sigma\end{aligned}$$

Thus for the twist distribution given above, α_{tip} has to equal $\frac{4C_T}{\sigma a}$ to produce a given thrust C_T. The lift coefficient distribution, c_l, then equals $\frac{4C_T}{\sigma x}$. Two ideas follow: (1) the inflow distribution is $\lambda = \sqrt{\sigma x c_l/8} = \sqrt{C_T/2}$. This is the uniform inflow expression as obtained earlier using the momentum theory. Recall that momentum theory gives the absolute minimum power that must be supplied to the rotor to sustain a given thrust. Thus the above twist requires minimum induced power. (2) $\theta_{tip} = \frac{4C_T}{\sigma a} + \phi_{tip} = \frac{4C_T}{\sigma a} + \sqrt{C_T/2}$. Thus the twist depends on one particular C_T value. The twist distribution, as it minimizes induced power, is called ideal twist, and such a rotor an ideal rotor. Note that it is ideal only for a given C_T. If C_T changes it no longer remains ideal. For example, if a higher (or lower) C_T is required a constant pitch must be added (or subtracted) to the hyperbolic distribution. This makes the inflow distribution non-uniform again.

A similar case is that of an optimum rotor. An optimum rotor, given as Case IV below, seeks to minimize both induced and profile power at the same time. Again, it is optimum only for a given thrust level. Minimum induced power can be achieved only if the inflow is forced to be uniform $\lambda = \sqrt{C_T/2}$. The question is, what should be the form of twist $\theta(x)$ that would minimize profile power in addition to induced power.

Case IV : Choose $\theta(x) = \alpha_0 + \frac{\lambda}{x}$, where α_0 is an unknown. λ is known, and must be uniform with value $\sqrt{C_T/2}$ in order to minimize induced power.

$$\begin{aligned}
\alpha(x) &= \theta(x) - \frac{\lambda}{x} \\
&= \text{constant } = \alpha_0 \\
c_l(x) &= \text{constant } = a\alpha_0
\end{aligned}$$

Now equate the inflow expressions and solve for solidity

$$\lambda = \sqrt{\frac{\sigma(x) x a \alpha_0}{8}} = \sqrt{\frac{C_T}{2}}$$

Thus the solidity must be choosen such that it equals

$$\sigma(x) = \frac{4C_T}{a\alpha_0} = \frac{\sigma_{tip}}{x}$$

This value of solidity will realize the minimize induced power criteria. The only unknown that remains is α_0. However, we know that this is the angle of attack all sections will operate in. What angle of attack do we want the sections to operate in ? Such, that the profile power is minimized. Using the expression for profile power obtained above, and remembering that the sectional drag c_d remains constant along the span (because the angle of attack remains constant α_0) we have

$$\begin{aligned}
C_{P0} &= \frac{1}{2}\int_0^1 \sigma(x) c_d x^3 dx \\
&= \frac{4C_T}{a\alpha_0}\int_0^1 c_d x^2 dx \\
&= \frac{2}{3} C_T \frac{c_d}{c_l}
\end{aligned}$$

So to minimize profile power, simply choose α_0 such that it maximizes C_l/C_d based on airfoil property data. Once this α_0 has been choosen, the geometric properties of the optimum rotor are set as

$$\begin{aligned}
\sigma(x) &= \frac{1}{x}\frac{4C_T}{a\alpha_0} \\
\theta(x) &= \alpha_0 + \frac{1}{x}\sqrt{\frac{C_T}{2}}
\end{aligned}$$

Solidity Ratio

To examine the performance of non-rectangular blades, we saw that the local solidity can be defined as

$$\sigma(r) = \frac{N_b c(r)}{\pi R}$$

where c(r) is the local chord at station r and N_b is total number of blades. For rectangular blades, the overall solidity, σ, is the same as the local solidity, σ. For non-rectangular blades, often, there is a needs to define an equivalent solidity, σ_e. That is, what would be the solidity of a rectangular blade that is equivalent to a given non-uniform blade ? Then the question is, equivalent in what sense ? Generates same thrust ? Or requires same power ? Naturally then, there are two types of equivalent solidities, thrust basis and power basis. The power basis is based on profile power. First equate the following two expressions

$$\begin{aligned} C_T &= \frac{1}{2}\sigma_e \int_0^1 c_l x^2 dx = \frac{1}{2}\int_0^1 \frac{N_b c(x)}{\pi R} c_l x^2 dx \\ C_{P0} &= \frac{1}{2}\sigma_e \int_0^1 c_d x^3 dx = \frac{1}{2}\int_0^1 \frac{N_b c(x)}{\pi R} c_d x^3 dx \end{aligned}$$

Then assume c_l, c_d to be constant over span to obtain

$$\begin{aligned} \sigma_e &= \tfrac{3N_b}{\pi R}\textstyle\int_0^1 cx^2\, dx && \text{thrust basis } (x = \tfrac{r}{R}) \\ \sigma_e &= \tfrac{4N_b}{\pi R}\textstyle\int_0^1 cx^3\, dx && \text{power basis} \end{aligned}$$

The equivalent solidity is used for performance comparison of two different rotors. They are of limited importance however, because of the following assumptions : (1) the sectional coefficients remain constant over span, and (2) the sectional coefficients would remain the same between the real and equivalent rotors. In reality, none of them hold true. The best way to compare two rotors is simply to compare their power requirements at the same thrust, or their Figure of Merits.

Taper Ratio

Linear variation of solidity is sometimes expressed as a taper ratio. For linearly tapering planform, the taper ratio is defined as root chord over tip chord.

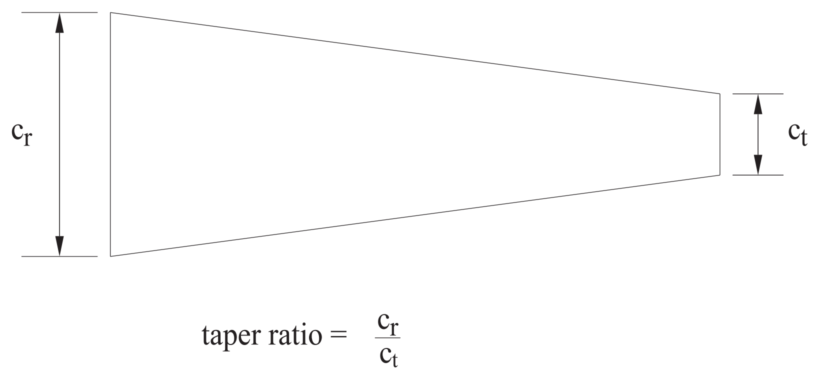

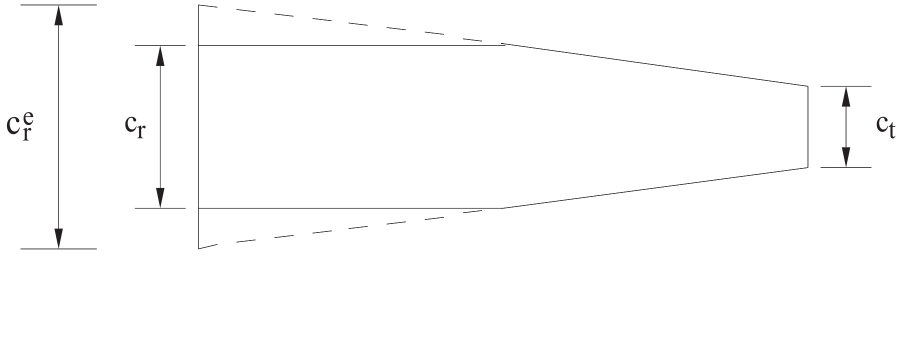

For partial linear tapered planform

$$\text{taper ratio} = \frac{\text{extended root chord}}{\text{tip chord}} = \frac{c_r^e}{c_t}$$

For large diameter rotors, the taper appears viable for performance gains.

1.1.2 Axial Climb

Upto now only the hover condition was considered. The analysis of axial climb and descent are shown using momentum theory, and combined blade element momentum theory. The theories, as before, are methods to related rotor inflow to rotor thrust.

Axial climb: Momentum theory

The fluid flow around the rotor looks very similar to that of hover, except that now a constant downwash, V_c is superimposed on the velocities. Thus the total far upstream, disk, and far downstream velocities are now $0 + V_c$, $v_i + V_c$, and $w + V_c$ respectively. Again, as in the case of hover, the thrust T can be easily related to the far downstream induced velocity w, using a momentum balance. The next step is then to simply relate w to v_i. This is done using energy balance. It can be shown that w is again equal to $2v_i$. The slipstream contraction then, follows obviously from mass balance. The steps are shown below.

In hover, the energy balance was formulated by conserving total pressure. It can also be formulated easily by conserving kinetic energy. The kinetic energy of the fluid moving out of the control volume per unit time is $\frac{1}{2}\dot{m}(v_c + w)^2$. The kinetic energy moving in per unit time is $\frac{1}{2}\dot{m}v_c^2$. The balance is the work done on the fluid per unit time, i.e., thrust times the displacement of the fluid per unit time $T(v_c + v_i)$. Thus

$$\begin{aligned} T(v_c + v_i) &= \frac{1}{2}\dot{m}(v_c + w)^2 - \frac{1}{2}\dot{m}v_c^2 && \text{energy balance} \\ \text{T} &= \dot{m}(v_c + w) - \dot{m}v_c = \dot{m}w && \text{momentum balance} \end{aligned}$$

Using the second expression in the first equation it follows, $w = 2v_i$.

Keeping in mind $\dot{m} = \rho A(v_c + v_i)$, we have $T = \rho A(v_c + v_i)w$. This can be expressed either in terms of only v_i or w. Thus $T = 2\rho A v_i(v_c + v_i) = \rho A w(v_c + w/2)$. The first expression is usually used to directly relate v_i to T. Often, instead of T, v_i is related to the hover induced velocity, i.e., what v_i would be in case of hover. Recall, that v_i in case of hover is related to thrust by the relation $v_h^2 = \frac{T}{2\rho A}$. Thus we have

$$v_h^2 = (v_c + v_i)v_i$$

It follows

$$\frac{v_i}{v_h} = -\frac{v_c}{2v_h} \pm \sqrt{\left(\frac{v_c}{2v_h}\right)^2 + 1}$$

The positive sign provides the physically meaningful solution, as v_i should always be positive, i.e, downwards, for a positive thrust T upwards. The power required to climb, as a fraction of power required to hover, is simply

$$\frac{P}{P_h} = \frac{P_i + P_c}{P_h} = \frac{T(v_i + v_c)}{T v_h} = \frac{v_i}{v_h} + \frac{v_c}{v_h} = \frac{v_c}{2v_h} \pm \sqrt{\left(\frac{v_c}{2v_h}\right)^2 + 1}$$

where the positive sign provides the physically meaningful solution.

Consider a case when the rate of climb is such that $v_c/v_h << 2$.

$$
\begin{aligned}
\frac{v_i}{v_h} &\cong -\frac{v_c}{2v_h} + 1 \\
v_i &\cong v_h - \frac{1}{2}v_c \\
P_i &= T(v_h - \frac{1}{2}v_c) + Tv_c + P_0 \\
&= Tv_h + P_0 + T\frac{v_c}{2} \\
&= P_h + T\frac{v_c}{2} \qquad \text{assuming profile power remains same as in hover}
\end{aligned}
$$

This means that the increased power required for steady climb is half the rate of change of potential energy. Which means that if the maximum power of an aircraft is P_{max}, and the hover power is P_h, then a steady rate of climb of twice the excess power to thrust ratio can be established, $v_c = 2(P_{max} - P_h)/T$. This approximation holds as long as the rate of climb remains much lesser compared to the hover induced velocity.

Note that the initial climb rate is $(P_{max} - P_h)/T$, but a final steady-state climb rate of twice this value can be reached. This is because the induced velocity in steady climb is reduced by twice the climb velocity from induced velocity in hover.

Axial climb: Combined Blade Element Momentum theory

We have for an annulus

$$
\begin{aligned}
dT &= \rho(2\pi r dr)(v_c + v_i)(2v_i - 0) \\
dC_T &= 4\lambda(\lambda - \lambda_c)x dx
\end{aligned}
$$

where

$$
\begin{aligned}
\lambda &= \frac{v_c + v_i}{\Omega R} \\
\lambda_c &= \frac{v_c}{\Omega R}
\end{aligned}
$$

Then equate dC_T Blade Element theory and Momentum theory

$$
\frac{1}{2}\sigma a \left(\theta - \frac{\lambda}{x}\right) x^2 dx = 4\lambda(\lambda - \lambda_c)x dx
$$

Solve for λ as a function of x

$$
\lambda(x) = \sqrt{A^2 + B\theta x} - A \tag{1.3}
$$

where

$$
\begin{aligned}
A &= \frac{\sigma a}{16} - \frac{\lambda_c}{2} \\
B &= \frac{\sigma a}{8}
\end{aligned}
$$

1.1.3 Axial Descent

Descending flight is similar to ascent, except that v_c is negative. For example, a descent of 5 m/s can be viewed as an ascent of -5 m/s. However the same expressions as ascent cannot be used.

Note that in all three conditions, hover, ascent, and descent the thrust must act upwards. Thus the force on the fluid must be downwards. The control volumes therefore have a similar geometry, constricted below the rotor and expanded above. In all three cases the rotor pushes the fluid down. However, during descent, unlike in hover and climb, the freestream velocity is from below the rotor. As a result, the fluid, in response to the rotor pushing it down, slows down or decelerates above the rotor. The far upstream, disk, and far downstream velocities are still v_c, $v_c + v_i$, and $v_c + w$, except far upstream is now below the rotor, and far downstream is above the rotor.

Axial descent: Momentum theory

Define positive direction to be downwards.

$$\begin{aligned} T(v_c + v_i) &= \frac{1}{2}\dot{m}(v_c)^2 - \frac{1}{2}\dot{m}(v_c + w)^2 && \text{energy balance} \\ \mathrm{T} &= \dot{m}(v_c) - \dot{m}(v_c + v_i) = -\dot{m}w && \text{momentum balance} \end{aligned}$$

Using the second expression in the first equation it follows, $w = 2v_i$.

Following the same procedure as in axial climb we have

$$\begin{aligned} T &= -\dot{m}w = -2\rho A(v_c + v_i)v_i \\ v_h^2 &= -(v_c + v_i)v_i \end{aligned}$$

It follows

$$\frac{v_i}{v_h} = -\frac{v_c}{2v_h} \pm \sqrt{\left(\frac{v_c}{2v_h}\right)^2 - 1}$$

The negative sign provides the physically meaningful solution. The power required to climb, as a fraction of power required to hover, is simply

$$\frac{P}{P_h} = \frac{P_i + P_c}{P_h} = \frac{T(v_i + v_c)}{Tv_h} = \frac{v_i}{v_h} + \frac{v_c}{v_h} = \frac{v_c}{2v_h} \pm \sqrt{\left(\frac{v_c}{2v_h}\right)^2 - 1}$$

where the negative sign provides the physically meaningful solution.

Axial climb: Combined Blade Element Momentum theory

We have for an annulus

$$\begin{aligned} dT &= -\rho(2\pi r dr)(v_c + v_i)(2v_i - 0) \\ dC_T &= -4\lambda(\lambda - \lambda_c)x dx \end{aligned}$$

where

$$\begin{aligned} \lambda &= \frac{v_c + v_i}{\Omega R} \\ \lambda_c &= \frac{v_c}{\Omega R} \end{aligned}$$

Then equate dC_T Blade Element theory and Momentum theory

$$\frac{1}{2}\sigma a\left(\theta - \frac{\lambda}{x}\right)x^2 dx = -4\lambda(\lambda - \lambda_c)x dx$$

Solve for λ as a function of x

$$\lambda(x) = \sqrt{A^2 + B\theta x} - A \tag{1.4}$$

where

$$\begin{aligned} A &= \frac{\sigma a}{16} + \frac{\lambda_c}{2} \\ B &= -\frac{\sigma a}{8} \end{aligned}$$

1.1.4 Forward Flight

In hovering flight, there is an axial symmetry of airflow, whereas, in forward flight there is no axial symmetry of airflow. There is a periodic aerodynamic environment. For an anti-clockwise rotation from the top, the blades on the starboard side advances into the oncoming airflow, and the blades on the port side retreates from it.

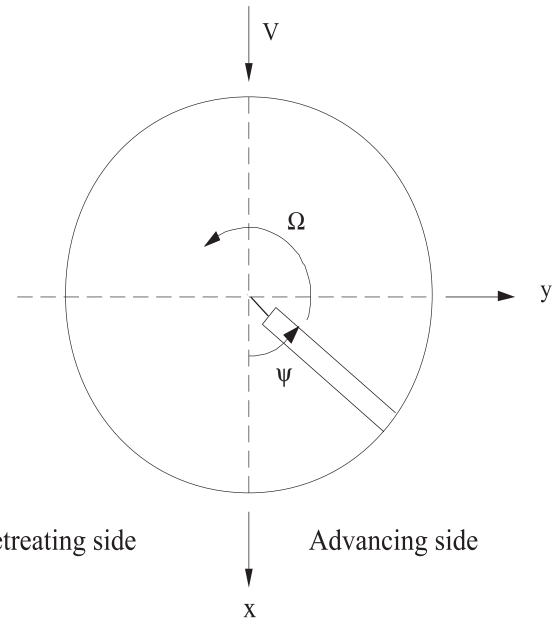

Clearly is a greater velocity of airflow on the advancing side of the disk as compared to the retreating side. This results in periodic variation of air loads on the blade. Left to themselves, the blades would generate more lift on the advancing side than on the retreating side and the aircraft would roll over to the left. The remedy is to put a flap hinge at the blade root, so that the blades can freely flap up about the hinge, without rolling the whole aircraft over. The idea was suggested by Charles Renard (1904), patented by Louis Breguet (1908), and applied successfully by Juan de la Cierva on the autogyro (1923). When the blades are allowed to flap, the problem is now reversed. For a lifting rotor, transitioning from hover to forward flight, the aircraft now rolls to the right. We shall see later why. The remedy is to introduce a mechanism for cyclic pitch variations along with a flap hinge. The roll moment can now be completely controlled. In addition to flapping, the other important blade motions are lag and torsion. The lag motion is extremely important for aero-elastic stability. The elastic twist is extremely important for aero-elastic loads. The blade motions are created in response to the airloads. In turn, the motions change the trajectory of the blades in space, and determine the airloads. During a steady flight, the variation of airloads are periodic. Even though the airloads vary with azimuth, they vary in exactly the same manner over every rotor revolution. During unsteady flights, like evasive turns, rolling pull-outs, pull-up, diving turns, and other maneuvers, the airloads are not periodic. We shall consider only steady flight in this chapter.

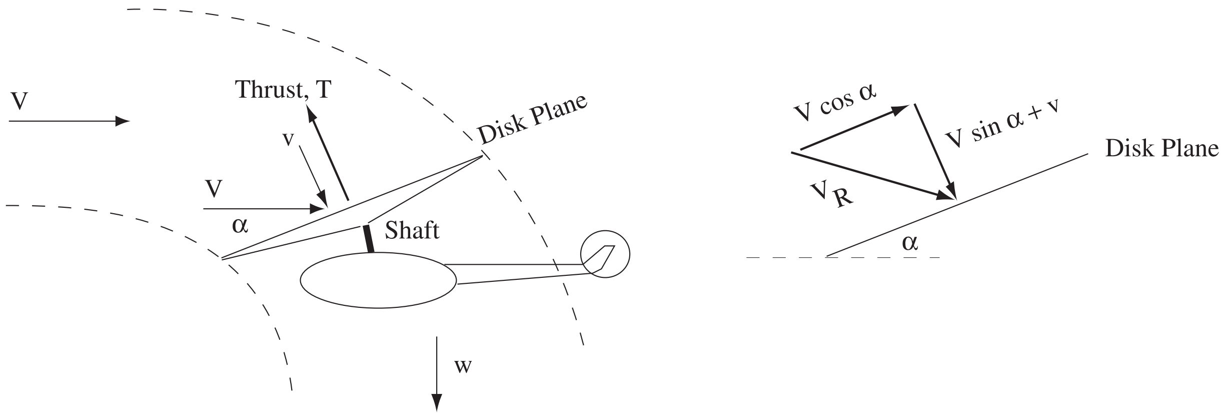

Figure 1.2: **Flow around a rotor in forward flight**

Momentum theory : Glauert's combination

Glauert (1926) combined momentum theory in hover with forward flight theory of fixed wings. A thin planer wing with elliptical loading has an induced drag given by

$$D_i = \frac{T^2}{2\rho A V^2}$$

The induced power and power to thrust ratio then becomes

$$\begin{aligned} P_i &= D_i V \\ &= \frac{T^2}{2\rho A V} \\ \frac{P_i}{T} &= \frac{T}{2\rho A V} \end{aligned}$$

Now replace P_i/T with v_i from the rotor result. This gives

$$\begin{aligned} v_i &= \frac{T}{2\rho A V} \\ T &= 2\rho A v_i V \end{aligned}$$

According to Glauert, for a rotor in forward flight replace V with $\sqrt{(V\cos\alpha)^2 + (V\sin\alpha + v_i)^2}$ to have

$$T = 2\rho A v_i \sqrt{(V\cos\alpha)^2 + (V\sin\alpha + v_i)^2}$$

The goal was simply to achieve the following: at high speed $v_i \cong 0$, we get back fixed wing result $T = 2\rho A v_i V = 2\rho A(P_i/T)V = 2\rho A(D_i V/T)V$; at low speed $V = 0$, we get back rotor hover result $T = 2\rho A v_i^2$.

Thus, Glauert postulated the momentum theory for forward flight by mathematically connecting the fixed wing and the hovering rotor results. The theory satisfies the outer limits (end conditions) and strangely, it is satisfactory even for intermediate flight conditions.

Momentum theory: Physical interpretation

A physical interpretation of Glauert's theory is as follows. Figure 1.2 shows the flow around the rotor disk in forward flight.

V = forward speed of the helicopter

v = normal induced velocity at the disk

w = far wake induced velocity

α = disk tilt

then, in keeping with the axial flow results, the induced velocity at the far wake is assumed to be twice the induced velocity at the disk.

$$\begin{aligned} w &= 2v \\ T &= \dot{m}2v \\ \dot{m} &= \rho A V_R \end{aligned}$$

where V_R is the resultant velocity through the disk, see figure 1.2.

$$\begin{aligned} V_R &= \sqrt{(V\cos\alpha)^2 + (V\sin\alpha + v)^2} \\ T &= 2\rho A v\sqrt{(V\cos\alpha)^2 + (V\sin\alpha + v)^2} \end{aligned}$$

Now define advance ratio μ and inflow ratio λ as follows.

$$\begin{aligned} \mu &= \frac{V\cos\alpha}{\Omega R} = \frac{\text{tangential velocity at the disk}}{\text{Tip velocity}} \\ \lambda &= \frac{V\sin\alpha + v}{\Omega R} = \frac{\text{Normal velocity at the disk}}{\text{Tip velocity}} \\ \lambda &= \mu\tan\alpha + \lambda_i \end{aligned}$$

Typically $\mu = 0.25$ to 0.4 and λ_i is of order 0.01 where $\lambda_i = \frac{v}{\Omega R}$, induced inflow ratio. Non-dimensionalising the thrust expression we have

$$\begin{aligned} C_T &= 2\lambda_i\sqrt{\lambda^2 + \mu^2} \\ \lambda_i &= \frac{C_T}{2\sqrt{\lambda^2 + \mu^2}} \\ \lambda_i &= \frac{\lambda_h^2}{\sqrt{\lambda^2 + \mu^2}} \end{aligned}$$

Thus the inflow equation becomes

$$\lambda = \mu\tan\alpha + \frac{C_T}{2\sqrt{\lambda^2 + \mu^2}}$$

The inflow equation is nonlinear and therefore an iteration procedure is used to solve it. Johnson suggested a Newton-Raphson solution scheme,

$$\lambda_{n+1} = \lambda_n - (f/f')_n$$

where

$$f(\lambda) = \lambda - \mu \tan\alpha - \frac{c_T}{2} \frac{1}{\sqrt{\mu^2 + \lambda^2}}$$

Therefore

$$\begin{aligned} \lambda_{n+1} &= \lambda_n - \frac{\lambda_n - \mu \tan\alpha - \frac{C_T}{2}(\mu^2 + \lambda_n^2)^{\frac{1}{2}}}{1 + \frac{C_T}{2}(\mu^2 + \lambda_n^2)^{-\frac{3}{2}}\lambda_n} \\ &= \left(\frac{\mu \tan\alpha + \frac{c_T}{2} \frac{(\mu^2 + 2\lambda^2)}{(\mu^2+\lambda^2)^{3/2}}}{1 + \frac{c_T}{2} \frac{\lambda}{(\mu^2+\lambda^2)^{3/2}}} \right)_n \end{aligned}$$

Usually 3 to 4 iterations are enough to achieve a converged solution. Figures 1.3 and 1.4 show example solutions of this equation with changing thrust levels, and shaft tilt angle.

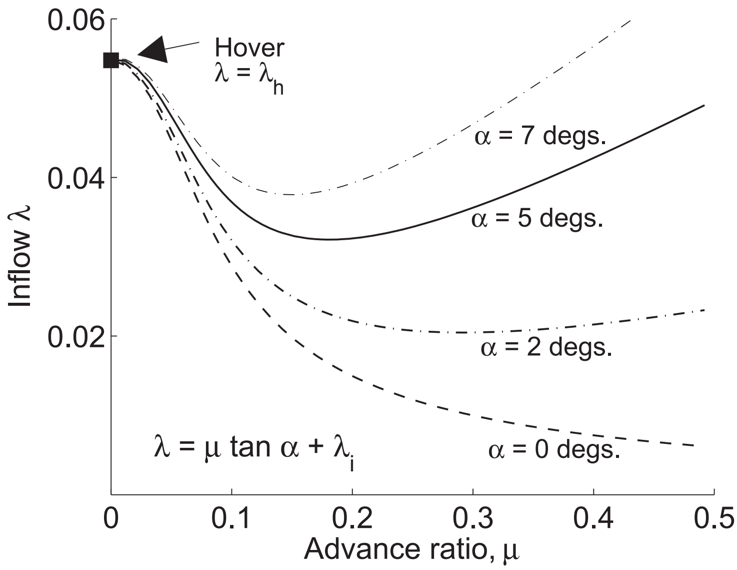

Figure 1.3: **Inflow variation with forward speed for different disk tilt angles;** $C_T = 0.006$

Note that, in the induced inflow expression given earlier

$$\lambda_i = \frac{\lambda_h^2}{\sqrt{\mu^2 + \lambda^2}}$$

λ_h can, in general, be modified with the empirical correction factor $\kappa_p \sqrt{C_T}/2$. κ_p is often replaced with a different correction factor in forward flight κ_f.

$$\begin{aligned} \lambda_i &= \mu \tan\alpha + \frac{\kappa_f C_T/2}{\sqrt{\mu^2 + \lambda^2}} \\ &\cong \mu \tan\alpha + \kappa_f \frac{C_T}{2\mu} \qquad \text{valid for } \mu > 1.5\lambda_h \end{aligned}$$

Thus, the effect of forward flight is to reduce induced velocity as a result of increased mass flow through the disk and thus reduce the induced power. The result is based on the assumption of uniform inflow over the entire disk. In reality, the induced power may increase at high speeds due to nonuniform inflow.

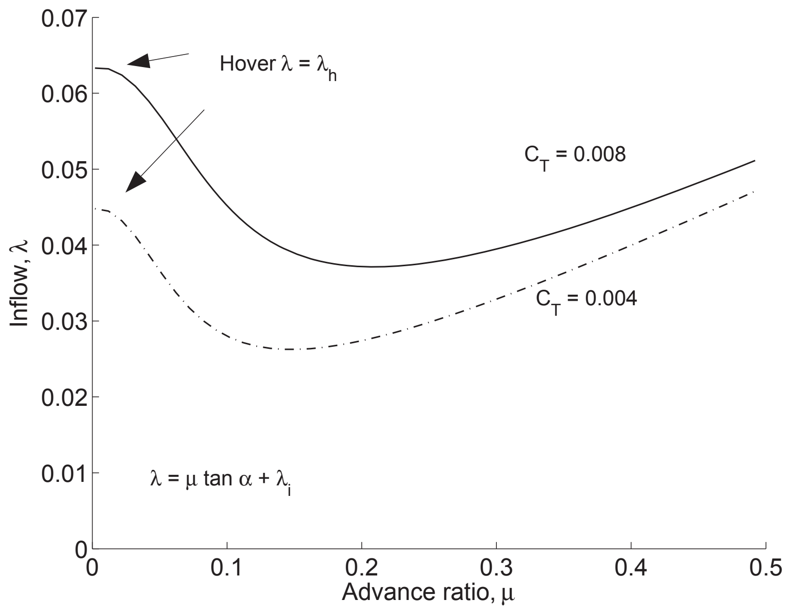

Figure 1.4: **Inflow variation with forward speed for different thrust levels;** $\alpha = 5^o$

The blade element theory for forward flight is quite similar to the one discussed for hover flight, except that the flow components, u_t, u_p, are modified. Consider a model rotor in a wind tunnel with shaft held fixed vertically. Assume that the blades are not allowed any other motion but rotation. This can be called a rigid rotor. The airflow velocity at a radial station r is $\Omega r + V \sin\psi$ where V is the incoming wind velocity and Ω is the rotational speed. Thus the non-dimensional sectional air velocities are

$$\begin{aligned} u_t &= x + \mu \sin\psi \\ u_p &= \lambda \\ u_r &= \mu \cos\psi \end{aligned}$$

The advancing blade encounters higher velocity than the retreating blade. If the pitch is held fixed, the lift on the advancing side is greater than that on the retreating side. This creates periodic bending moments at the root of the blade which rolls the rotor from the advancing side towards the retreating side, i.e. roll left for counter clockwise rotation. For example, the sectional lift, in non-dimensional form, is

$$\begin{aligned} \frac{dF_z}{\rho ca(\Omega R)^2 R} &\cong \frac{dL}{\rho ca(\Omega R)^2 R} \\ &= \frac{1}{2}(\theta u_t^2 - u_p u_t)dx \\ &= \frac{1}{2}(\theta x^2 + 2x\mu\theta \sin\psi + \theta\mu^2 \sin^2\psi - \lambda x - \mu\lambda \sin\psi)dx \\ &= \left(\theta\frac{x^2}{2} + \theta\frac{\mu^2}{4} - \frac{\lambda x}{2}\right) + \left(\theta\mu x - \frac{\lambda x}{2}\right)\sin\psi + \left(-\theta\frac{\mu^2}{4}\right)\cos 2\psi \end{aligned}$$

In the simple example above, the lift has a constant part, a $\sin\psi$ part and a $\cos 2\psi$ part. The constant part is called the steady lift. The $\sin\psi$ part is called 1 per revolution (1/rev, or 1p) lift. It is an oscillatory lift which completes one cycle of variation over one rotor revolution, i.e., it completes one cycle of variation as the blade moves from $\psi = 0$, through $\psi = 90, 180, 270$ degrees back to $\psi = 360 = 0$ degrees. At $\psi = 0$ it has a value of 0, at $\psi = 90$ degrees it reaches the maximum value $\theta\mu x - \frac{\lambda x}{2}$, at $\psi = 180$ degrees it is again 0, at $\psi = 270$ degrees it reaches the minimum value $-(\theta\mu x - \frac{\lambda x}{2})$, and finally back to 0 at $\psi = 360$. Similarly the $\cos 2\psi$ part is called 2/rev lift. The bending moment produced by the lift at the root of the blade is

$$\begin{aligned} \frac{dM}{\rho ca(\Omega R)^2 R^2} &= \frac{rdL}{\rho ca(\Omega R)^2 R^2} \\ &= \left(\theta\frac{x^3}{2} + \theta\frac{\mu^2}{4}x - \frac{\lambda x^2}{2}\right) + \left(\theta\mu x^2 - \frac{\lambda x^2}{2}\right)\sin\psi + \left(-\theta\frac{\mu^2}{4}x\right)\cos 2\psi \end{aligned}$$

which is simply the lift expression multiplied by x. The net bending moment at the shaft is obtained by simply integrating the above expression over the span.

$$\begin{aligned} M &= \frac{1}{\rho ac\Omega^2 R^4}\int_0^R r\, dF_z \\ &= \left(\frac{\theta}{8} + \theta\frac{\mu^2}{8} - \frac{\lambda}{6}\right) + \left(\theta\frac{\mu}{3} - \frac{\lambda}{6}\right)\sin\psi + \left(-\theta\frac{\mu^2}{8}\right)\cos 2\psi \end{aligned}$$

M is the aerodynamic root moment. Like lift it has a steady and two oscillatory components. Note that the root moment occurs at the blade root and has a direction perpendicular to the blade span. As the blade rotates around the azimuth, the direction of the root moment rotates along with the blade. Therefore the root moment is also termed hub rotating moment. The rotating moment can be resolved along two fixed axes, say the aircraft roll and pitch axes. The resolved moments do not change in direction and are called the hub fixed moments. The roll and pitch moments are

$$\begin{aligned} M_R &= +M\sin\psi && \text{positive to left} \\ M_P &= -M\cos\psi && \text{positive nose up} \end{aligned}$$

This leads to 2 important concepts. First, Note that the hub fixed moments are hub rotating moments multiplied with a 1/rev variation. Thus a steady rotating moment generates a 1/rev hub fixed moment. A 1/rev rotating moment generates steady and 2/rev hub fixed moments. A 2/rev rotating moment generates 1/rev and 3/rev hub fixed moments, and so on. In general, a N/rev rotating moment generates $N \pm 1/rev$ hub fixed moments. Our M_β expression had steady, 1 and 2/rev. Therefore our M_R and M_P expressions would have a highest harmonic of 3/rev. Assume M_R to have the following general form.

$$M_R(\psi) = m_0 + m_1\sin(\psi + \phi_1) + m_2\sin(2\psi + \phi_2) + m_3\sin(3\psi + \phi_3)$$

where the phase lags ϕ_1, ϕ_2, and ϕ_3 are introduced to account for both sin and cos components of the harmonics.

Now, imagine there are three identical blades. The root moments from each will be identical, except shifted in phase by $360/3 = 120$ degrees. This is because when blade 1 is at $\psi = 0$, blade 2 is at $\psi = 120$, and blade 3 is at $\psi = 240$ degrees, where ψ is always referred with respect to blade 1. Physically it means that at $\psi = 0$ the root moment is made up of three contributions. Contribution 1 is from blade 1 at $\psi = 0$. Contribution 2 is from blade 2. The value of this contribution is exactly same as the root moment blade 1 would have when it reaches $\psi = 120$ degrees. Thus, the contribution from blade 2 is easily found by putting $\psi = 120$ degrees in the expression for blade 1 root moment. Similarly, contribution 3 is from blade 3, and it is easily found by putting $\psi = 240$ degrees in the expression for blade 1 root moment. The concept applies to hub fixed moments as well. When blade 1 contributes $M_R(\psi)$ as a hub fixed load, blade 2 contributes $M_R(\psi + 120)$, and blade 3 contributes $M_R(\psi + 240)$. All three contributions are added at the hub. The end result from simple trigonometry is only steady and 3/rev.

$$\begin{aligned} M_R(\psi)_{total} &= (M_R)_{blade1} + (M_R)_{blade2} + (M_R)_{blade3} \\ &= M_R(\psi) + M_R(\psi + 120) + M_R(\psi + 240) \\ &= 3m_0 + 3m_3(3\psi + \phi_3) \end{aligned}$$

In general, for N_b blades, the fixed frame moments (and forces in general) are always steady, and pN_b/rev components where p is an integer.

High 1/rev blade root moments, and the high steady hub fixed moment that it generates was a major cause of early rotor failures. The question is quite natural, how to minimize this oscillatory bending moment at the root and how to reduce the aircraft rolling moment. The advent of flap hinge (Renard - 1904) relieved the blade root moment, by allowing the blades to flap freely in response to oscillatory aerodynamic flap moments.

1.2 Basic Structural Dynamics

The dynamics of a single degree of freedom system is reviewed. It is then applied to a simple rotor blade flapping model.

1.2.1 Second-Order Systems

Consider a second-order ordinary differential equation describing the motion of a mass spring system.

$$m\ddot{q} + kq = f(t)$$

where q describes the motion, and $\ddot{q}$ is the second derivative with respect to time t. $Q(t)$ is the external forcing. The motion exhibited by the mass m in absence of external forcing is called *natural motion.* Such is the case when the mass is given an initial displacement or velocity and then released. The motion is then governed by the *homogenous equation*

$$m\ddot{q} + kq = 0$$

where the forcing $f(t)$ is set to zero. We seek a solution of the following type.

$$q(t) = Ae^{st}$$

Substituting in the equation we have

$$(ms^2 + k)A = 0$$

$A = 0$ yields a trivial solution $q = 0$. For a non-trivial solution, one must have

$$ms^2 + k = 0$$

which leads to

$$s = \pm i\sqrt{k/m} = i\omega_n$$

where

$$\omega_n = \sqrt{k/m}$$

Thus the governing equation allows a solution of the above type only for these two values of s. These are called the *eigen-values* and ω_n (rad/s) the natural frequency of the system. The homogenous solution is then

$$q(t) = A_1 e^{i\omega_n t} + A_2 e^{-i\omega_n t} \tag{1.5}$$

The physical interpretation of the solution can be found using the Euler's theorem. Euler's theorem states

$$e^{\pm i\omega t} = \cos\omega t \pm i\sin\omega t$$

It follows from above

$$\begin{aligned} e^{i\pi/2} &= i; \quad e^{-i\pi/2} = -i \\ e^{i\pi} &= -1; \quad e^{-i\pi} = 1 \end{aligned} \tag{1.6}$$

The term $A_1 e^{i\omega_n t}$ can now be physically interpreted. the first term is expanded as

$$A_1 e^{i\omega_n t} = A_1 \cos\omega_n t + iA_1 \sin\omega_n t \tag{1.7}$$

The two resulting terms $A_1 \cos\omega_n t$ and $A_1 \sin\omega_n t$ are simply the projections of a rotating vector of magnitude A_1 along two mutually perpendicular axes. The rotation speed is ω_n radians/second, and the vector is initially aligned with the horizontal axis. In this sense $A_1 e^{i\omega_n t}$ represents a rotating vector. Similarly $A_2 e^{-i\omega_n t}$ represents another rotating vector. It has magnitude A_2 and rotates with the same speed ω rad/s, but, rotates in a direction opposite to $A_1 e^{i\omega_n t}$. This is easily seen from below.

$$A_2 e^{-i\omega_n t} = A_2 \cos\omega_n t - iA_2 \sin\omega_n t = A_2 \cos(-\omega_n t) + iA_2 \sin(-\omega_n t) \tag{1.8}$$

It follows that an expression of the form $A_1 e^{\pm i(\omega_n t+\phi)}$, where ϕ is a constant, represents a pair of counter-rotating vectors (corresponding to the '+' and '−' signs), which are always ahead of the vectors $A_1 e^{\pm i\omega_n t}$ by an angle ϕ in the direction of their respective rotations. ϕ is called a phase angle. The horizontal and vertical directions are simply two orthogonal directions; one of them can be chosen arbitrarily. Conventionally they are referred to as the Real and Imaginary directions.

The time derivative of $q(t)$ in eqn. 1.5 yields the following expression for velocity

$$\dot{q}(t) = A_1 i\omega_n e^{i\omega_n t} + iA_2(-i)\omega_n e^{-i\omega_n t} \tag{1.9}$$

which, using the expressions for i and $-i$ from eqns. 1.6 produce

$$\dot{q}(t) = A_1\omega_n e^{i(\omega_n t+\pi/2)} + iA_2\omega_n e^{-i(\omega_n t+\pi/2)} \tag{1.10}$$

Thus the expression for velocity represents two counter-rotating vectors of magnitudes $A_1\omega_n$ and $A_2\omega_n$ which rotate ahead of the displacement vectors by $\pi/2$ in the direction of their respective rotations. Thus the velocities are ahead of the displacement by a phase angle of $\pi/2$ radians. Similarly the expression for acceleration represents two counter-rotating vectors which lead velcity vectors by $\pi/2$ radians in phase, and therefore the displacement vectors by π.

$$\begin{aligned} \ddot{q}(t) &= A_1 i^2\omega_n^2 e^{i\omega_n t} + A_2(-i)^2\omega_n^2 e^{-i\omega_n} \\ &= A_1\omega_n e^{i(\omega_n t+\pi)} + iA_2\omega_n e^{-i(\omega_n t+\pi)} \end{aligned} \tag{1.11}$$

To summarize, each of the two terms in eqn. 1.5 represents two projections of a rotating vector along two perpendicular directions. Each projection defines a harmonic oscillator. The combination of the two counter-rotating vectors leads to two harmonic oscillators of different magnitudes along the Real (or cosine) and Imaginary (or sine) axes.

$$p(t) = (A_1 + A_2)\cos\omega_n t + i(A_1 - A_2)\sin\omega_n t \tag{1.12}$$

This implies that the physical displacement of the mass m is a combination of cosine and sine harmonics of different amounts, and could be expressed in the following form

$$q(t) = A\sin\omega_n t + B\cos\omega_n t \tag{1.13}$$

It can also be expressed in a pure sine form by substituting $A = \sin\phi_1$ and $B = \cos\phi_1$

$$q(t) = C\sin(\omega_n t + \phi_1); \quad C = \sqrt{A^2 + B^2}; \quad \phi_1 = \tan^{-1}(A/B) \tag{1.14}$$

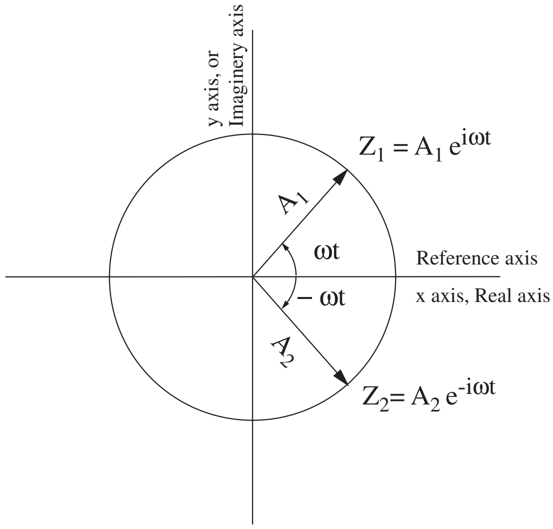

Figure 1.5: **Projections of rotating vectors along orthogonal axes produce harmonic motion**

or in a pure cosine form by substituting $A = \cos\phi_2$ and $B = \sin\phi_2$

$$q(t) = C\cos(\omega_n t - \phi_2); \quad C = \sqrt{A^2 + B^2}; \quad \phi_2 = \tan^{-1}(B/A) \tag{1.15}$$

They are identical, i.e. they yield exactly the same value at a given time t, as $\tan^{-1}(A/B) + \tan^{-1}(B/A) = \pi/2$. Two unknown constants appear in every form which are determined from the initial conditions $q(0), \dot{q}(0)$. These are the intial displacement and velocities. The final solution is called the natural response of the system. It represents perpetual motion in response to an initial perturbation.

In reality systems contain damping. Response to an initial perturbation decays depending on the amount of damping. Consider a real system with damping c in Newtons per m/s.

$$m\ddot{q} + c\dot{q} + kq = f(t) \tag{1.16}$$

For natural response, set $f(t) = 0$, and solve the resulting homogenous equation. For convenience the equation is divided by m and expressed in the following form

$$\ddot{q} + 2\xi w_n \dot{q} + w_n^2 q = 0$$

Note that k/m has been expressed in terms of the natural frequency of the system (derived earlier). c/m has been replaced with a damping ratio ξ which changes with w_n even if the physical damper c remains same. $c/m = 2\xi\omega_n$. As before, we seek a solution of the form $q = Ae^{st}$. Substituting in the differential equation we obtain

$$s = (-\xi \pm \sqrt{\xi^2 - 1})\omega_n$$

Case 1: $\xi = 0$ undamped
Roots same as shown earlier, imaginary.

$$s = \pm i\omega_n$$

Case 2: $\xi = 1$ critically damped
Equal roots, real and negative.

$$\begin{aligned} s_1 &= -\omega_n \\ s_2 &= -\omega_n \end{aligned}$$

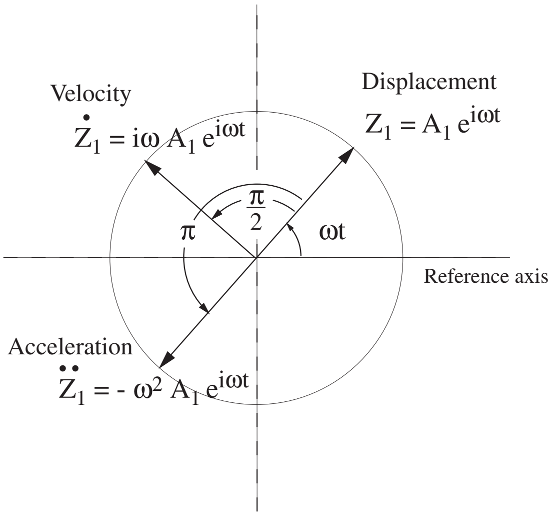

Figure 1.6: **The rotating vectors representing velocity and acceleration lead the displacement by $\pi/2$ and π radians**

In case of repeated roots the solution is of a slightly different from than the rest

$$\begin{aligned} q(t) &= A_1 e^{-\omega_n t} + A_2 t e^{-\omega_n t} \\ &= (A_1 + A_2 t) e^{-\omega_n t} \end{aligned}$$

Case 3: $\xi > 1$ over damped
Unequal roots, real and negative

$$s_{1,2} = (-\xi \pm \sqrt{\xi^2 - 1})\omega_n$$

$$\begin{aligned} q(t) &= A_1 e^{s_1 t} + A_2 e^{s_2 t} \\ &= e^{-\xi\omega_n t}(A_1 e^{\sqrt{\xi^2 - t\omega_n t}} + A_2 e^{-\sqrt{\xi^2 - t\omega_n t}}) \end{aligned}$$

Case 4: $0 < \xi < 1$
The above were all special cases, for a realistic system the damping coefficient is less than one. In this case $\sqrt{\xi^2 - 1}$ is imaginary, and better expressed as $i\sqrt{1 - \xi^2}$. Thus,

$$s_{1,2} = (-\xi \pm i\sqrt{1 - \xi^2})\omega_n$$

$$\begin{aligned} q(t) &= e^{-\xi\omega_n t}(A_1 e^{i\sqrt{1-\xi^2}\omega_n t} + A_2 e^{-i\sqrt{1-\xi^2}\omega_n t}) \\ &= e^{-\xi\omega_n t} A \cos(\sqrt{1 - \xi^2}\omega_n t - \phi) \end{aligned}$$

A and ϕ are two arbitrary constants that can be determined from the initial conditions. The damped frequency w_d is given by

$$w_d = \sqrt{1 - \xi^2}\omega_n$$

The decay envelope of the oscillatory response in case 4 is given by

$$E(\xi, \omega_n, t) = e^{-\xi\omega_n t}$$

In summary, the solution to

$$\ddot{q} + 2\xi\omega_n \dot{q} + \omega_n^2 q = 0$$

is given by

$$\begin{aligned} q(t) &= e^{-\xi\omega_n t} A\cos(\sqrt{1-\xi^2}\omega_n t - \phi) && 0 < \xi < 1 \\ &= A\cos(\omega_n t - \phi) && \xi = 0 \\ &= \text{ no oscillations} && \xi \geq 0 \end{aligned}$$

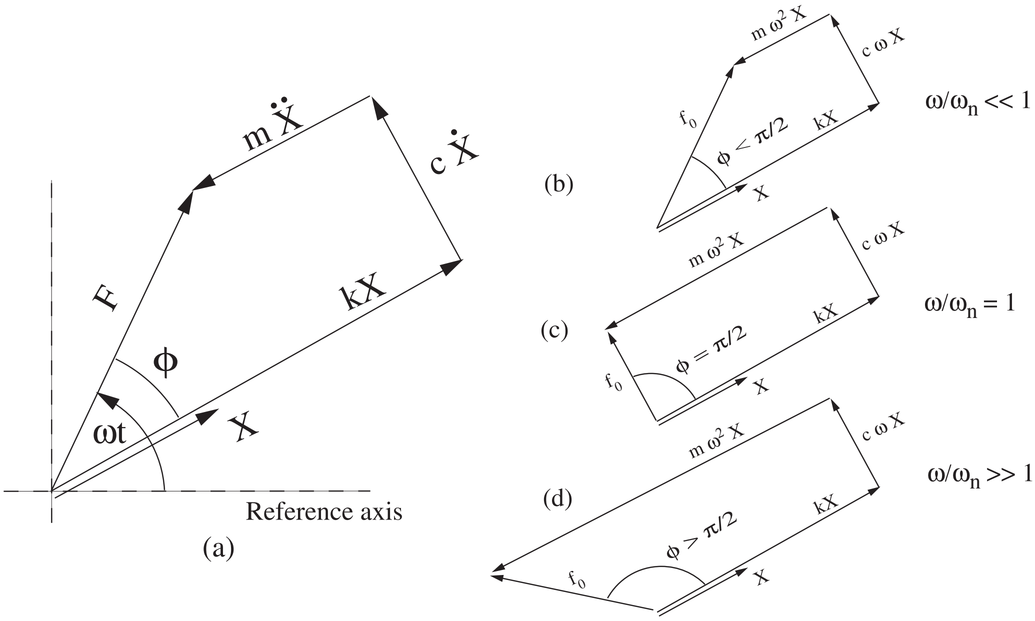

Figure 1.7: **(a) General relationship between spring force, damper force, inertia force and external force in forced vibration; (b) when $\omega/\omega_n << 1$ both inertia and damper force small, ϕ small; (c) when $\omega/\omega_n = 1$ damper force equal and opposite to external force, inertial equal and opposite to spring force, $\phi = \pi$; (d)$\omega/\omega_n >> 1$ external force almost equal to inertial force, ϕ approaches π**

Now consider the forced response of the system. Here we want to solve the *inhomogenous* system as given by eqn. 1.16. Let the external forcing be $f(t) = f_0 \cos\omega t$. The equation then takes the following form.

$$m\ddot{q} + c\dot{q} + kq = f_0 \cos\omega t$$

It is easy to check by substitution that the equation accepts a solution of the form

$$q(t) = c_1 \cos\omega t + c_2 \sin\omega t$$

i.e. the response is at the same frequency as that of the forcing, ω. Note that, here we have taken the forcing to be the real axis projection of a rotating vector. One can use both projections by representing the forcing as $f(t) = f_0 e^{i\omega t}$. The form of the solution should then be taken as $q(t) = ce^{i(\omega t - \phi)}$. The real (or imaginary) part of the solution would then be exactly same as the solution obtained by using the real (or imaginary) part of the forcing expressions alone.

c_1 and c_2 (or c, if one performs the calculations using the complex notation) are not arbitrary constants, as earlier in the case of natural response. Forced response of a linear system does not depend on initial conditions. The magnitude of forcing f_0 can be written as ka, where k is the spring stiffness, and a a displacment. Expressing f_0 as $f_0 = ka$ and dividing throughout by m we have

$$\ddot{q} + 2\xi\omega_n\dot{q} + \omega_n^2 q = \omega_n^2 a \cos\omega t$$

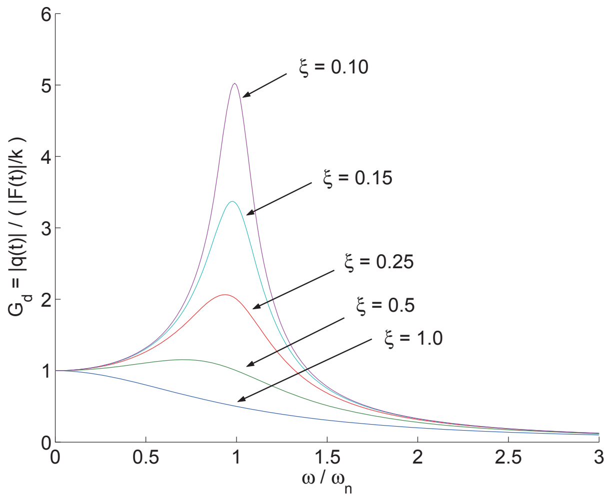

Figure 1.8: **Transfer function between forcing and displacement**

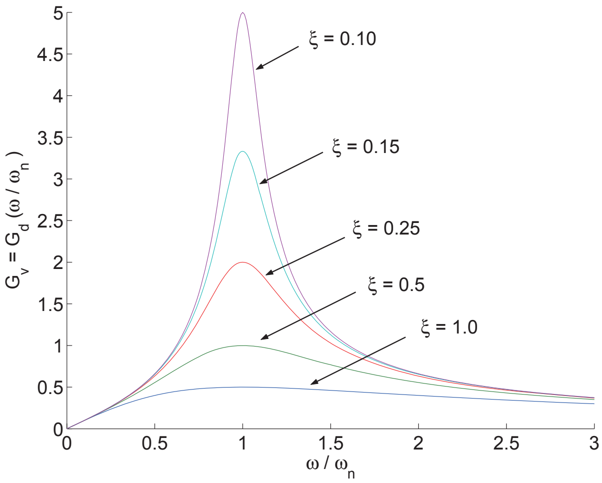

Figure 1.9: **Transfer function between forcing and velocity**

Substitute $q(t)$ in the equation, and determine c_1 and c_2 by equating the cos and sin components (for complex domain calculations equate the real and imaginery parts to find c and ϕ). The final solution has the following form.

$$
\begin{aligned}
q(t) &= \frac{f_0/k}{\sqrt{\left[1-\left(\frac{\omega}{\omega_n}\right)^2\right]^2+\left[2\xi\frac{\omega}{\omega_n}\right]^2}}\cos(\omega t-\phi) \quad := \quad a\mathbf{G_d}\cos(\omega t-\phi) \\
\phi &= \tan^{-1}\frac{2\xi\frac{\omega}{\omega_n}}{1-\left(\frac{\omega}{\omega_n}\right)^2}
\end{aligned}
$$

where ϕ is the phase angle by which the displacement lags the forcing. The ratio of the magnitude of displacement to the magnitude of forcing is a transfer function

$$
\frac{|q|}{|f|}=\frac{a\mathbf{G_d}}{f_0}=\frac{a\mathbf{G_d}}{ka}
$$

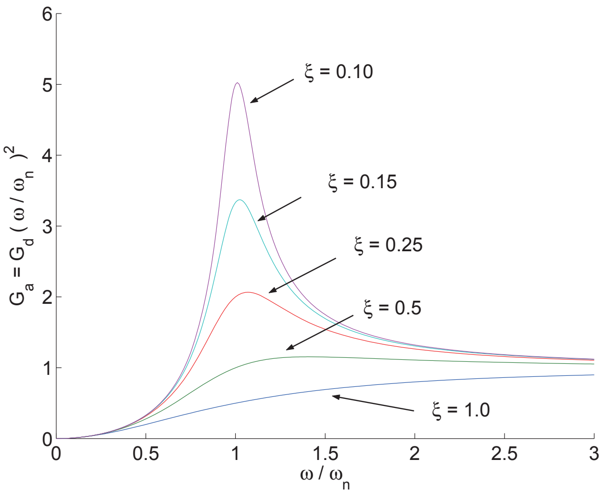

Figure 1.10: **Transfer function between forcing and acceleration**

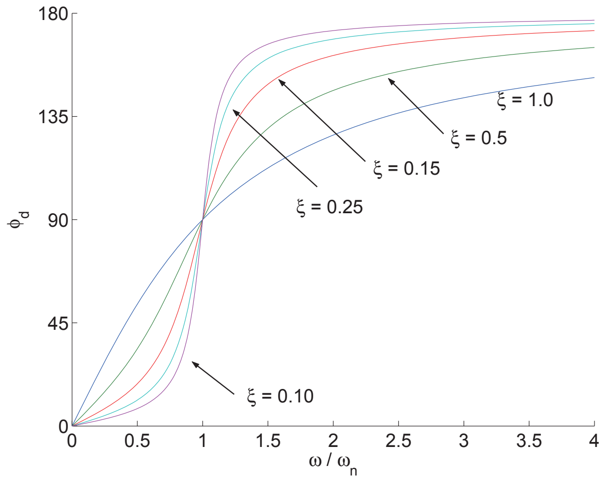

Figure 1.11: **Phase by which response (displacement) lags forcing**

Re-arrange to obtain

$$\frac{|q|}{|f|/k} = \mathbf{G}_d$$

The numerator of the left hand side is the maximum displacement including dynamics. The denominator of the left hand side is the maximum displacement ignoring dynamics. Thus the ratio gives a magnification factor due to the dynamics. This can be termed the displacement gain function, $\mathbf{G}_d$. $\mathbf{G}_d$ is a function of ω/ω_n and ξ.

For $\xi = 0$ and $\omega/\omega_n = 1$ we have an infinite response. Physically, the response blows up in time domain. The equation and the solution take the following form.

$$\begin{aligned} \ddot{q} + \omega_n^2 q &= \omega_n^2 a \cos \omega_n t \\ q(t) &= \frac{a}{2}\omega_n t \cos(\omega_n t - \pi/2) \end{aligned}$$

The velocity-force, and acceleration-force transfer functions are $|\dot{q}|/|F|$ and $|\ddot{q}|/|F|$. To express them as functions of ω/ω_n non-dimensionalize as

$$\begin{aligned}
\frac{|\dot{q}|}{\frac{|f|}{k}\omega_n} &= \mathbf{G}_d \frac{\omega}{\omega_n} = \mathbf{G}_v \\
\frac{|\ddot{q}|}{\frac{|f|}{k}\omega_n^2} &= \mathbf{G}_d \left(\frac{\omega}{\omega_n}\right)^2 = \mathbf{G}_a
\end{aligned}$$

Note that the denominator of the left hand side expression for $\mathbf{G}_a$ represents the rigid body acceleration of m in absence of dynamics. To obtain the phase by which the velocity and acceleration lags the forcing, differentiate the response

$$\begin{aligned}
\dot{q}(t) &= -a\mathbf{G}_d\omega\sin(\omega t - \phi) = a\mathbf{G}_d\omega\cos(\omega t - [\phi - \pi/2]) = a\mathbf{G}_d\omega\cos(\omega t - \phi_v) \\
\ddot{q}(t) &= a\mathbf{G}_d\omega\cos(\omega t - [\phi - \pi]) = a\mathbf{G}_d\omega\cos(\omega t - \phi_a)
\end{aligned}$$

It follows, as we expect

$$\begin{aligned}
\phi_v &= \phi - \pi/2 \\
\phi_a &= \phi - \pi
\end{aligned}$$

The displacement, velocity, and acceleration transfer functions are shown in figures 1.8, 1.9, and 1.10. The displacement phase lag with respect to forcing is shown in figure 1.11.

The total response of the system, for a realistic case, then becomes

$$q(t) = e^{-\xi\omega_n t} A\cos(\sqrt{1-\xi^2}\omega_n t - \phi) + \frac{a}{\sqrt{\left[1 - \left(\frac{\omega}{\omega_n}\right)^2\right]^2 + \left[2\xi\frac{\omega}{\omega_n}\right]^2}}\cos(\omega t - \phi)$$

By realistic case, it is assumed that $0 \le \xi < 1$, and $\omega \ne \omega_n$ if $\xi = 0$.

The first part is the initial condition response. The second part is the steady state response. In case of numerical integration both are obtained as part of the solution. If the periodic response is desired, one must wait till the initial condition response dies down. For high damping, the initial condition response dies down quickly. For low damping, it takes a long time. For zero damping it remains forever. Methods like Harmonic Balance and Finite Element in Time are used to obtain the steady state solution in such cases, when the steady state solution is desired uncontaminated with the initial condition response.

1.2.2 Reduction to First-Order Form

The second-order eqn. 1.16 can be reduced to first-order form by the substitution

$$x_1 = q, \quad x_2 = \dot{q}$$

It follows

$$\dot{x}_1 = \dot{q} = x_2$$

$$\dot{x}_2 = \ddot{q} = (-c/m)x_2 + (-k/m)x_1 + (1/m)f$$

leading to

$$\begin{pmatrix} \dot{x}_1 \\ \dot{x}_2 \end{pmatrix} = \begin{bmatrix} 0 & 1 \\ -k/m & -c/m \end{bmatrix} \begin{pmatrix} x_1 \\ x_2 \end{pmatrix} + \begin{pmatrix} 0 \\ f/m \end{pmatrix}$$

In matrix notation

$$\dot{\mathbf{x}} = \mathbf{A}\mathbf{x} + \mathbf{f} \tag{1.17}$$

$\mathbf{x}$ is the vector of *states* describing the system and $\mathbf{f}$ is a vector of excitations. For a general second-order system with n degrees of freedom, $q_1, q_2, \ldots, q_n$, eqn. 1.16 becomes

$$\mathbf{M}\ddot{\mathbf{q}} + \mathbf{C}\dot{\mathbf{q}} + \mathbf{K}\mathbf{q} = \mathbf{F}$$

The corresponding first-order system now has a state vector $\mathbf{x}$ of size $2n$ containing $q_1, q_2, \ldots, q_n$ and $\dot{q}_1, \dot{q}_2, \ldots, \dot{q}_n$, with

$$\mathbf{A} = \begin{bmatrix} \mathbf{0} & \mathbf{I}_n \\ -\mathbf{M}^{-1}\mathbf{K} & -\mathbf{M}^{-1}\mathbf{C} \end{bmatrix} \quad \text{of size } \ 2n \times 2n$$

$$\mathbf{f} = \begin{bmatrix} \mathbf{0} \\ \mathbf{M}^{-1}\mathbf{F} \end{bmatrix} \quad \text{of size } \ 2n \times 1$$

The forcing $\mathbf{F}$ can be a superposition of m seperate excitations $u_1, u_2, \ldots, u_m$.

$$\mathbf{F} = \mathbf{G}\mathbf{u}$$

where $\mathbf{G}$ is of size $n \times m$. The first-order system then takes the following form

$$\dot{\mathbf{x}} = \mathbf{A}\mathbf{x} + \mathbf{B}\mathbf{u} \tag{1.18}$$

where $\mathbf{B}$ is now given as

$$\mathbf{B} = \begin{bmatrix} \mathbf{0} \\ \mathbf{M}^{-1}\mathbf{G} \end{bmatrix} \quad \text{of size } \ 2n \times m$$

In the previous section we had obtained transfer functions between q, $\dot{q}$ and f, directly using the solution of the second-order equation. The same transfer functions can also be obtained using the first-order eqn. 1.18. For this simple case, $n = m = 1$, $\mathbf{G} = 1$, $\mathbf{u} = f$, and

$$\mathbf{B} = \begin{bmatrix} 0 \\ 1/m \end{bmatrix}$$

Under many circumstances, often encountered in control theory, the second-order system has the following form

$$\ddot{\mathbf{q}} + \mathbf{A}'\dot{\mathbf{q}} + \mathbf{B}'\mathbf{q} = \mathbf{C}'\ddot{\mathbf{u}} + \mathbf{D}'\dot{\mathbf{u}} + \mathbf{E}'\mathbf{u}$$

where the forcing is a function of the excitation and its derivatives. The corresponding first-order form is given by

$$\mathbf{A} = \begin{bmatrix} \mathbf{0} & \mathbf{I}_n \\ -\mathbf{B}' & -\mathbf{A}' \end{bmatrix} \quad \text{of size } \ 2n \times 2n$$

$$\mathbf{B} = \begin{bmatrix} \mathbf{B_1} \\ \mathbf{B_2} \end{bmatrix} \quad \text{of size } \ 2n \times m$$

where

$$\mathbf{B_1} = \mathbf{D}' - \mathbf{A}'\mathbf{C}'$$

$$\mathbf{B_2} = \mathbf{E}' - \mathbf{A}'\mathbf{B_1} - \mathbf{B}'\mathbf{C}'$$

The states are defined as

$$\mathbf{x_1} = \mathbf{q} - \mathbf{C}'\mathbf{u}$$

$$\mathbf{x_2} = \dot{\mathbf{q}} - \mathbf{C}'\dot{\mathbf{u}} - \mathbf{B_1}\mathbf{u}$$

1.2.3 Rotor Blade Dynamics

The rotor blades undergo three dominant dynamic motions.

β : flap motion

normal to the plane of rotation

positive for upward motion

ζ : lag motion

motion in the plane of rotation

positive lag opposes rotation lead-lag is in opposite direction to lag-motion

θ : pitch motion

rotation of blade about elastic axis

positive for nose up motion

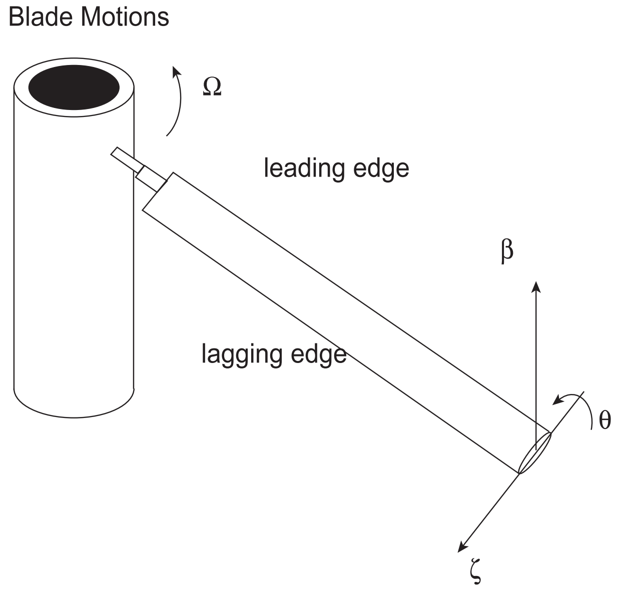

The flap motion of the blades, we shall see, relieves the root moments. The letting the blades flap freely, in response to lift, the blades are allowed to take up a certain orientation in space. The direction of the rotor thrust is determined by this orientation.

The flap motion will induce Coriolis moment in the lag direction. To relieve this lag moment at the root of the blade, a lag hinge is introduced.

The pitch motion is a blade dynamic response to aerodynamic pitching moments. The pitch control angle, $\theta_{con}(\psi)$, on the other hand, is a pilot input provided via a hub mechanism e.g. a pitch bearing or torque tube. Note that the net pitch angle at a blade section consists of three components: (1) pitch motion $\theta(r, \psi)$, (2) pitch control angle $\theta_{con}(\psi)$, and (3) the in-built twist $\theta_{tw}(r)$. The first component, pitch motion, is also called elastic twist. The second component, pitch control angle, is a means to control the direction of thrust vector. The blades are still free to flap, but they flap in response to a lift distribution which is influenced via the pitch control angles. Thus the blade orientation in space, and the resultant thrust direction can be controlled. The pitch control angles have a steady (called collective) and 1/rev components. The sin part of the 1/rev component is called the longitudinal cyclic, and the cos part is called the lateral cyclic.

The advent of cyclic pitch (Pescare - 1924) helped to control the thrust vector. The thrust vector can be oriented to the desired direction without changing the shaft orientation. Therefore, the inclusion of the flap hinge and the cyclic pitch converts a static problem into a dynamic one because the blade motion now becomes important.In this chapter we shall study the flap motion to understand the basic principles behind the rotor and moments generated by the rotor.

The next figure shows a typical articulated rotor blade with mechanical flap and lag hinges, and a pitch bearing.

For hingeless rotor, the mechanical flap and lag hinges are eliminated. Virtual hinges are introduced by making the the blade quite flexible structurally near the root so that it behaves as if there are hinges for flap and lag motions.

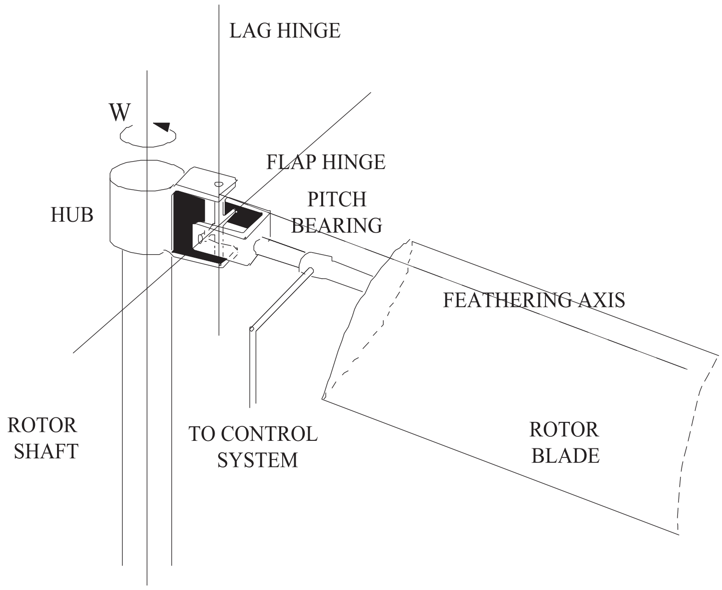

1.2.4 Flap motion of a rotor blade

Consider the general model where a blade flaps about a hinge located at a distance e from the shaft axis. See Fig. 6.2. The equation governing the blade flapping motion is obtained as follows

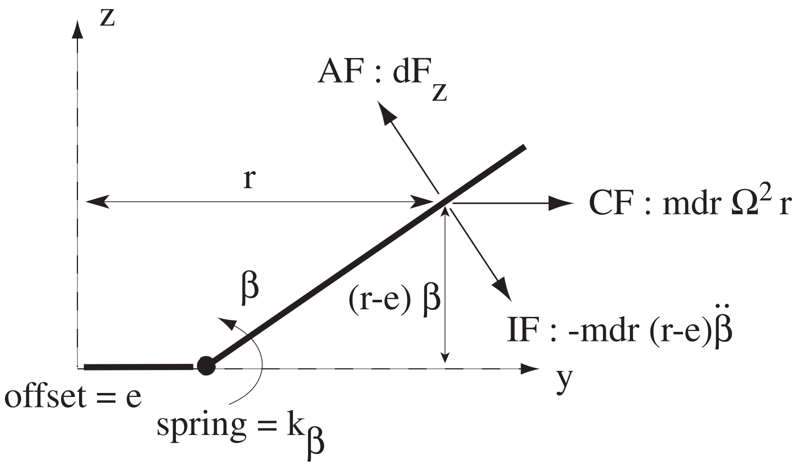

Figure 1.12: **Flapping motion about a hinge**

$$\text{External moments about hinge} = (\text{Blade inertia about hinge}).(\text{angular acceleration } \ddot{\beta})$$

The right hand side of the above equation can be defined as the negative of inertial moment about the hinge. Then we have

$$\begin{aligned} \text{External moments about hinge} &= -\text{Inertial moment about hinge} \\ \text{External moments about hinge} &+ \text{Inertial moment about hinge} = 0 \\ \text{Net moments about hinge} &= 0 \end{aligned}$$

The blade inertia about the hinge is $\int_e^R m(r-e)^2 dr$. Thus the inertial moment is $-\int_e^R m(r-e)^2 \ddot{\beta} dr$. This is a moment generated by the spanwise integration of a force $-m(r-e)\ddot{\beta}dr$ acting on an element of length dr. This is defined here as the inertial force (IF) on the element. The external moments are the moments generated by the aerodynamic force (AF) and the centrifugal force (CF), and the restoring spring moment. The moment due to aerodynamic force is $\int_e^R (r-e)dF_z$. The moment due to centrifugal force is $\int_e^R (mdr)\Omega^2 r(r-e)\beta$. The restoring spring moment is $k_\beta \beta$. The forces are shown in Fig. 6.2. The moment balance about the hinge is then as follows.

$$\int_e^R (r-e)dF_z - \int_e^R (mdr)\Omega^2 r(r-e)\beta - k_\beta\beta = \int_e^R m(r-e)^2\ddot{\beta}dr$$

which can be re-arranged to read

$$\int_e^R (r-e)dF_z - \int_e^R (mdr)\Omega^2 r(r-e)\beta - \int_e^R m(r-e)^2\ddot{\beta}dr = k_\beta\beta$$

Physically, the above equation means that the aerodynamic moment is cancelled partly by the centrifugal moment, used partly to generate acceleration in flap, and the remainder is balanced by the spring at the hinge. Thus the net balance of moments at the hinge is provided by the spring, where $k_\beta\beta$ is the spring moment. This quantity is called the hinge moment or the root moment. Note that, in the case of perfectly articulated blade with a free hinge, i.e. $k_\beta = 0$, then the balance of aerodynamic and centrifugal moments is used up entirely by the blade acceleration. The root moment in this case is forced to zero. For hingeless blades or articulated blades with a spring the root moment is $k_\beta\beta$. Often a pre-cone angle β_p pre-set to reduce the hinge moment. For example β_p could be an estimate of steady flap angle. The equation then becomes

$$\int_e^R rdF_z - \int_e^R (mdr)\Omega^2 r(r-e)\beta - \int_e^R m(r-e)^2\ddot{\beta}dr = k_\beta(\beta-\beta_p) \tag{1.19}$$

Define

$$\begin{aligned} I_\beta &= \int_e^R (r-e)^2 mdr \\ S_\beta &= \int_e^R (r-e)mdr \end{aligned}$$

The moment balance then becomes

$$k_\beta(\beta-\beta_p) = \int_e^R (r-e)dF_z - I_\beta\ddot{\beta} - \left(1 + \frac{eS_\beta}{I_\beta}\right)\Omega^2 I_\beta\beta \tag{1.20}$$

The above expression is important. It says that the root moment can be calculated either using the left hand side, or the right hand side. They are identical, and their equality generates the flap equation. The expression can be further simplified. First club the β terms together to obtain

$$I_\beta\ddot{\beta} + \left(1 + \frac{eS_\beta}{I_\beta} + \frac{k_\beta}{I_\beta\Omega^2}\right)\Omega^2 I_\beta\beta = \int_e^R (r-e)dF_z + k_\beta\beta_p$$

Then define $\left(1 + \frac{eS_\beta}{I_\beta} + \frac{k_\beta}{I_\beta \Omega^2}\right) = \nu_\beta^2$.

$$I_\beta \ddot{\beta} + \nu_\beta^2 \Omega^2 I_\beta \beta = \int_e^R (r-e) dF_z + k_\beta \beta_p$$

Divide by I_b. I_b is the inertia about the shaft axis, i.e.$\int_0^R r^2 m dr$. I_β was the inertia about the hinge. For practical purposes we make the assumption $I_\beta \cong I_b$. Thus we have

$$\ddot{\beta} + \nu_\beta^2 \Omega^2 \beta = \frac{1}{I_b} \int_e^R (r-e) dF_z + \frac{k_\beta}{I_\beta} \beta_p \tag{1.21}$$

The above equation determines flap dynamics and shows a natural frequency of $\nu_\beta \Omega$, equal to ω_β say. The unit of this frequency ω_β is radians per second. Note that the unit of Ω is itself radians per second. Thus ν_β is a non-dimensional number with no units. If it is 1, that means ω_β, the natural frequency of flap dynamics is simply Ω. Physically, it means that the flap degree of freedom, when excited, completes one full cycle of oscillation just when the blade finishes one full circle of rotation. Recall, that this type of motion, which completes one cycle just in time for one circle of rotation, is called a 1/rev motion. Thus the ν_β is 1/rev. It is a non-dimensional frequency such that a phenomenon at that frequency just has time to finish one cycle within one blade revolution. A ν_β of say 1.15/rev means, that the flap motion when excited finishes one cycle well within one complete blade rotation and has time for a bit more. It finishes 1.15 cycles within one blade rotation.

The dynamics with time can be recast into dynamics with rotor azimuth, a more physically insightful expression for rotor problems. Divide by Ω^2.

$$\frac{1}{\Omega^2} \ddot{\beta} + \nu_\beta^2 \beta = \frac{1}{I_\beta \Omega^2} \int_e^R (r-e) dF_z + k_\beta \beta_p$$

Now

$$\begin{aligned} \psi &= \Omega t \\ \ddot{\beta} &= \frac{\partial^2 \beta}{\partial t^2} = \Omega^2 \frac{\partial^2 \beta}{\partial \psi^2} = \Omega^2 \overset{**}{\beta} \end{aligned}$$

The equation takes the following form.

$$\overset{**}{\beta} + \nu_\beta^2 \beta = \gamma \overline{M_\beta} + \frac{\omega_{\beta_0^2}}{\Omega^2} \beta_p \quad \text{where} \quad \overset{**}{\beta} = \frac{\partial^2 \beta}{\partial \psi^2} \tag{1.22}$$

Equation (1.22) describes the evolution of flap angle as the blade moves around the azimuth ψ.

$$\begin{aligned} \gamma &= \frac{\rho a c R^4}{I_b} \\ \overline{M_\beta} &= \frac{1}{\rho c a (\Omega R)^2 R^2} \int_e^R (r-e) dF_z \\ \omega_{\beta_0^2} &= \frac{k_\beta}{I_\beta} \end{aligned}$$

γ is called Lock number. $\overline{M_\beta}$ is the aerodynamic flap moment in non-dimensional form. It is the same form as given earlier. ω_{β_0} is the non-rotating flap frequency. Note that it is zero in case of a perfect hinge with zero spring constant. ν_β is the rotating natural frequency of flap dynamics.

$$
\begin{aligned}
&\nu_\beta = \sqrt{1 + \frac{eS_\beta}{I_\beta} + \frac{k_\beta}{I_\beta \Omega^2}} && \text{non-dimensional in /rev} \\
&\omega_\beta = \Omega\sqrt{1 + \frac{eS_\beta}{I_\beta} + \frac{k_\beta}{I_\beta \Omega^2}} && \text{dimensional in radians/sec} \\
&S_\beta = \frac{1}{2}m(R-e)^2 && \text{for uniform blade} \\
&I_\beta = \frac{1}{3}m(R-e)^3 && \text{for uniform blade} \\
&\frac{eS_\beta}{I_\beta} \cong \frac{3}{2}\frac{e}{R}
\end{aligned}
\tag{1.23}
$$

Now consider the case where the flap hinge contains both a spring and a damper. Equation 1.20 is then modified to read

$$
k_\beta(\beta - \beta_p) + c_\beta \dot{\beta} = \int_e^R (r-e)dF_z - I_\beta \ddot{\beta} - \left(1 + \frac{eS_\beta}{I_\beta}\right)\Omega^2 I_\beta \beta \tag{1.24}
$$

which simply means that the balance of moment at the hinge is provided by the spring and damper moments. Following the same procedure, equation 1.21 modifies to

$$
\ddot{\beta} + \left(\frac{c_\beta}{I_\beta}\right)\dot{\beta} + \nu_\beta^2 \Omega^2 \beta = \frac{1}{I_b}\int_e^R (r-e)dF_z + \frac{k_\beta}{I_\beta}\beta_p \tag{1.25}
$$

Equation 1.22 modifies to

$$
\overset{**}{\beta} + \left(\frac{c_\beta}{I_b \Omega}\right)\overset{*}{\beta} + \nu_\beta^2 \beta = \gamma \overline{M_\beta} + \frac{\omega_{\beta_0^2}}{\Omega^2}\beta_p
$$

or

$$
\overset{**}{\beta} + (2\xi\nu_\beta)\overset{*}{\beta} + \nu_\beta^2 \beta = \gamma \overline{M_\beta} + \frac{\omega_{\beta_0^2}}{\Omega^2}\beta_p \tag{1.26}
$$

where $c_\beta / I_b\Omega$ is conveniently expressed as $2\xi\nu_\beta$. ν_β is the flap frequency. ξ is defined as the damping ratio. This is simply one possible way of expressing the damping. Physically it means

$$
\begin{aligned}
c_\beta &= 2\xi\nu_\beta I_b \Omega \\
&= 2\xi\omega_\beta I_b
\end{aligned}
$$

c_β is a physical damper value. It does not depend on operating conditions. The damping ratio ξ, on the other hand, depends on the operating condition Ω, and blade property I_b. In general any frequency can be chosen to determine a corresponding ξ, as long as the physical value c_β remains unchanged. For example, in terms of the non-rotating frequency c_β can be expressed as follows.

$$
c_\beta = 2\xi_{nr}\omega_{\beta 0} I_b
$$

This ξ_{nr} is different from the ξ above obtained using the rotating frequency, but the physical flap damper value c_β offcourse is the same.

1.3 Aero-elastic Response

Assume that a blade exhibits only flapping motion. Assume further a simple case when the blade has no pre–cone angle, no root–damper, i.e. β_p=0, ξ=0, and the flap hinge is at the center of rotation.

1.3.1 Flap response for non-rotating blades

First consider a stationary blade with no rotation. The flap equation 1.21 then becomes

$$\ddot{\beta} + \omega_{\beta 0}^2 \beta = 0$$

When perturbed the blade exhibits a motion

$$\beta(t) = A\cos(\omega_{\beta 0} t - \phi)$$

where A and ϕ are constants to be determined from the initial conditions $\beta(0)$ and $\dot{\beta}(0)$, and $\omega_{\beta 0} = \sqrt{k_\beta / I_\beta}$.

1.3.2 Flap response for rotating blades in vacuum

Now consider that the rotor is rotating in a vacuum chamber. There is a centrifugal force but no aerodynamic force. Equations 1.21 then becomes

$$\ddot{\beta} + \omega_{\beta}^2 \beta = 0$$

When perturbed the blade exhibits a motion

$$\beta(t) = A\cos(\omega_{\beta} t - \phi)$$

where A and ϕ are constants to be determined from the initial conditions $\beta(0)$ and $\dot{\beta}(0)$, and

$$\begin{aligned}
\omega_\beta &= \Omega\sqrt{1 + \frac{3}{2}\frac{e}{R} + \frac{\omega_{\beta 0}^2}{\Omega^2}} \\
&= \Omega\sqrt{1 + \frac{3}{2}\frac{e}{R}} && \text{if } \omega_{\beta 0} = 0 \text{ i.e. } k_\beta = 0 \\
&= \Omega, && \text{if } k_\beta = 0, \text{ and } e = 0
\end{aligned}$$

However, for a rotating blade it is more convenient to non-dimensionalize the governing differential equation with Ω^2 which, as derived earlier, leads to the following

$$\overset{**}{\beta} + \nu_\beta^2 \beta = 0$$

$$\beta(\psi) = A\cos(\nu_\beta \psi - \phi)$$

where A and ϕ are constants to be determined from the initial conditions $\beta(0)$ and $\overset{*}{\beta}(0)$, and

$$\begin{aligned}
\nu_\beta &= \sqrt{1 + \frac{3}{2}\frac{e}{R} + \frac{\omega_{\beta 0}^2}{\Omega^2}} \\
&= \sqrt{1 + \frac{3}{2}\frac{e}{R}} && \text{if } \omega_{\beta 0} = 0 \text{ i.e. } k_\beta = 0 \\
&= 1 && \text{if } k_\beta = 0, \text{ and } e = 0
\end{aligned}$$

1.3.3 Flap response in hover

Consider a rotor in a hover stand. Or a helicopter in hover. From equation 1.22 we have

$$\overset{**}{\beta} + \nu_\beta^2 \beta = \gamma \overline{M_\beta}$$

where the aerodynamic flap moment is given by

$$\begin{aligned}
\overline{M_\beta} &= \frac{1}{\rho c a (\Omega R)^2 R^2} \int_0^R (r-e) dF_z \\
&\cong \frac{1}{\rho c a (\Omega R)^2 R^2} \int_0^R r dF_z \qquad \text{simplifying assumption for small } e \\
&= \frac{1}{\rho c a (\Omega R)^2 R^2} \int_0^R r \frac{1}{2} \rho c c_l U_T^2 dr \\
&= \frac{1}{\rho c a (\Omega R)^2 R^2} \int_0^R r \frac{1}{2} \rho c a (\theta - \frac{U_P}{U_T}) U_T^2 dr \\
&= \frac{1}{2} \int_0^1 x(\theta u_t^2 - u_p u_t) dx
\end{aligned}$$

For hover we have

$$\begin{aligned}
U_T &= \Omega r \\
U_p &= \lambda \Omega R + r\dot{\beta}
\end{aligned}$$

Note that, compared to the simple blade element formulation given earlier, U_p now has an addition component $r\dot{\beta}$ from blade flapping. Thus the blade dynamics, or elastic deformation affects the aerodynamic forces. In non-dimensional form we have

$$\begin{aligned}
u_t &= x \\
u_p &= \lambda + x \overset{*}{\beta}
\end{aligned}$$

Assume θ to be constant in hover, θ_0. The aerodynamic hinge moment then becomes

$$\begin{aligned}
\overline{M_\beta} &= \frac{1}{2} \int_0^1 x(\theta_0 x^2 - x^2 \overset{*}{\beta} - \lambda x) dx \\
&= \frac{\theta_0}{8} - \frac{\lambda}{6} - \frac{\overset{*}{\beta}}{8}
\end{aligned}$$

The aero-elastic form of the flap equation then becomes

$$\overset{**}{\beta} + \frac{\gamma}{8} \overset{*}{\beta} + \nu_\beta^2 \beta = \gamma \left(\frac{\theta_0}{8} - \frac{\lambda}{6} \right)$$

The steady state solution is a constant

$$\beta_0 = \frac{\gamma}{\nu_\beta^2} \left(\frac{\theta_0}{8} - \frac{\lambda}{6} \right)$$

Suppose the pilot provides a 1/rev control input in addition to a collective θ_0

$$\begin{aligned}
\theta(t) &= \theta_0 + \theta_{1s} \sin \Omega t \\
\theta(\psi) &= \theta_0 + \theta_{1s} \sin \psi
\end{aligned}$$

The steady state response contains not only a constant term but also a periodic term.

$$\beta(\psi) = \beta_0 + A\sin(\psi - \phi)$$

The constant term is same as before. The magnitude and phase of the periodic term can be obtained from the expression derived earlier for single degree of freedom systems. We have

$$\begin{aligned} \omega_n &= \nu_\beta \\ \omega &= 1 \\ 2\xi\omega_n &= \frac{\gamma}{8} \end{aligned}$$

Using the above expressions we have

$$\begin{aligned} A &= \frac{\theta_{1s}}{\sqrt{\left(\nu_\beta^2 - 1\right)^2 + \left(\frac{\gamma}{8}\right)^2}} \\ \phi &= \tan^{-1}\frac{\frac{\gamma}{8}}{\nu_\beta^2 - 1} \\ &= \frac{\pi}{2} - \tan^{-1}\frac{\nu_\beta^2 - 1}{\frac{\gamma}{8}} \end{aligned}$$

Thus the maximum flap response occurs almost 90° after maximum forcing. For $\nu_\beta = 1$, ϕ exactly 90°. Generally ν_β is slightly greater than one. Then ϕ is close to, but slightly lower than 90°. The flap solution is

$$\beta(\psi) = \frac{\gamma}{\nu_\beta^2}\left(\frac{\theta_0}{8} - \frac{\lambda}{6}\right) + \frac{\theta_{1s}}{\sqrt{\left(\nu_\beta^2 - 1\right)^2 + \left(\frac{\gamma}{8}\right)^2}}\sin\left(\psi - \frac{\pi}{2} + \tan^{-1}\frac{\nu_\beta^2 - 1}{\frac{\gamma}{8}}\right)$$

Assume $\nu_\beta = 1$. Then,

$$\begin{aligned} \beta(\psi) &= \gamma\left(\frac{\theta_0}{8} - \frac{\lambda}{6}\right) + \frac{8\theta_{1s}}{\gamma}\sin(\psi - \frac{\pi}{2}) \\ &= \gamma\left(\frac{\theta_0}{8} - \frac{\lambda}{6}\right) + \left(-\frac{8\theta_{1s}}{\gamma}\right)\cos\psi \\ &= \gamma\left(\frac{\theta_0}{8} - \frac{\lambda}{6}\right) + \beta_{1c}\cos\psi \end{aligned}$$

β_{1c} is, by definition, the cosine component of the flap response. Here $\beta_{1c} = (-8\theta_{1s})/\gamma$. Note that a sine input to the controls produce a cosine response in flap and vice-versa. This is simply because the flap motion occurs in resonance to the applied forcing, and therefore has a 90° phase lag with respect to it. This is the case for rotors with flap frequency exactly at 1/rev. For slightly higher flap frequencies, a sine input generates both a cosine as well as a sine output. However, as long as the flap frequency is near 1/rev (e.g. 1.15/rev for hingeless rotors, and 1.05/rev for articulated rotors), a sine input generates a dominant cosine output, and vice-versa.

1.3.4 Flap response in forward flight

Consider a rotor in a wind tunnel, or in forward flight. In forward flight the sectional velocity components vary with azimuth. The pitch variation in forward flight is of the form

$$\theta(r,\psi) = \theta_0 + \theta_{tw}\frac{r}{R} + \theta_{1c}\cos\psi + \theta_{1s}\sin\psi \qquad (1.27)$$

where θ_0, θ_{1c}, and θ_{1s} are called trim control inputs. They are provided to influence the steady and first harmonic flap response. The total flap response in forward flight contains a large number of harmonics.

$$\beta(\psi) = \beta_0 + \beta_{1c}\cos\psi + \beta_{1s}\sin\psi + \text{ higher harmonics} \tag{1.28}$$

For simplicity, let us consider only the first harmonics for the time being. Retaining only the first harmonics are often adequate for performance evaluations of a helicopter. By performance we mean rotor power, lift, drag, and aircraft trim attitudes. We shall study aircraft trim in a later section. Here, let us first see the sectional velocity components. Then the blade element forces. And then calculate the flap response.

The airflow components at a section are shown in the following figures.

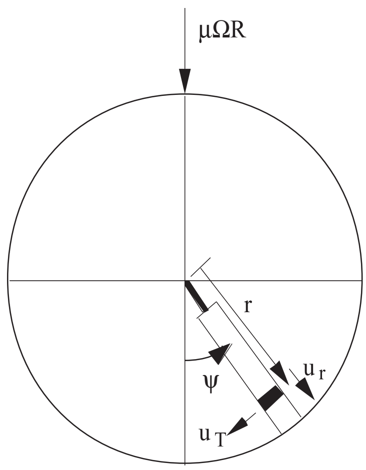

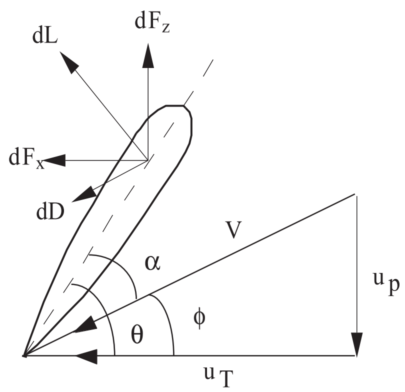

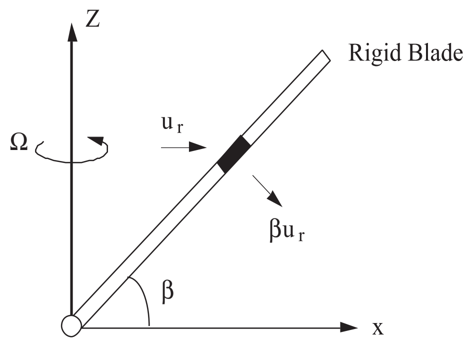

$$\phi = \frac{U_P}{U_T}$$
$$\Gamma = \frac{U_R}{U_T}$$

where Γ is the incident yaw angle at the section. The sectional drag acts along this angle. U_T and U_P are the tangential and perpendicular velocity components at a section. U_R is radial, not along the blade. Along the blade, and perpendicular to the blade components of U_R would be

$$U_R\cos\beta = \mu\Omega R\cos\psi\cos\beta$$
$$U_R\sin\beta = \mu\Omega R\cos\psi\sin\beta$$

Let us define the inflow $\lambda\Omega R$ to be positive downwards acting along the Z axis. The Z axis is aligned parallel to the rotor shaft. Then the mutually perpendicular velocity components at each section are

$$U_T = \Omega r + \mu\Omega R \sin\psi$$

$$U_P = \lambda\Omega R \cos\beta + r\dot{\beta} + \mu\Omega R \cos\psi \sin\beta$$

$$U_R = \mu\Omega R \cos\psi$$

U_S is the spanwise component acting along the blade. Assume $\cos\beta \cong 1$ and $\sin\beta \cong \beta$. Non-dimensionalize the velocity components w.r.t ΩR to obtain:

$$\frac{u_t}{\Omega R} = x + \mu \sin\psi$$

$$\frac{u_p}{\Omega R} = \lambda + x \overset{*}{\beta} + \beta\mu\cos\psi$$

$$\frac{u_r}{\Omega R} = \mu\cos\psi$$

The blade forces are

$$\begin{aligned} dF_z &= (dL\ \cos\phi - dD\ \sin\phi)\cos\beta \\ &\cong dL \qquad \text{because } dD \cong 0.1dL \\ &= \frac{1}{2}\rho c a U_T^2 \left(\theta - \frac{U_P}{U_T}\right) dr \\ &= \frac{1}{2}\rho c a\, dr\ \left(U_T^2\theta - U_P U_T\right) \end{aligned} \tag{1.29}$$

$$\begin{aligned} dF_x &= dL\ \sin\phi + dD\ \cos\phi\cos\Gamma \\ &\cong dF_z\frac{U_P}{U_T} + dD \\ &= \frac{1}{2}\rho c a U_T^2 \left(\theta - \frac{U_P}{U_T}\right)\frac{U_T}{U_P}dr + \frac{1}{2}\rho c a U_T^2 C_d dr \\ &= \frac{1}{2}\rho c a\, dr\ \left(U_P U_T\theta - U_P^2 + \frac{C_d}{a}U_T^2\right) \end{aligned} \tag{1.30}$$

$$\begin{aligned} dF_r &= -dL\sin\beta + dD\sin\Gamma \\ &\cong -\beta dL \\ &= -\beta\frac{1}{2}\rho c a\, dr\ \left(U_T^2\theta - U_P U_T\right) \end{aligned} \tag{1.31}$$

The aerodynamic flap moment is then

$$
\begin{aligned}
\overline{M_\beta} &= \frac{1}{\rho a c \Omega^2 R^4}\int_0^R r\,dF_z \\
&= \frac{1}{2}\int_0^1 x\left[\left(\frac{u_T}{\Omega R}\right)^2\theta - \left(\frac{u_p}{\Omega R}\right)\left(\frac{u_T}{\Omega R}\right)\right]dx \\
&= \frac{1}{2}\int_0^1 x\left(u_t^2\theta - u_p u_t\right)dx \\
&= \left(\frac{1}{8}+\frac{\mu}{3}\sin\psi+\frac{\mu^2}{4}\sin^2\psi\right)(\theta_0+\theta_{1c}\cos\psi+\theta_{1s}\sin\psi) \\
&\quad + \theta_{tw}\left(\frac{1}{10}+\frac{\mu^2}{6}\sin^2\psi+\frac{\mu}{4}\sin\psi\right) - \lambda\left(\frac{1}{6}+\frac{\mu}{4}\sin\psi\right) \\
&\quad - \overset{*}{\beta}\left(\frac{1}{8}+\frac{\mu}{6}\sin\psi\right) - \mu\beta\cos\psi\left(\frac{1}{6}+\frac{\mu}{4}\sin\psi\right)
\end{aligned}
$$

Recall the flap equation (1.22)

$$
\overset{**}{\beta} + \nu_\beta^2\beta = \gamma\overline{M_\beta} + \frac{\omega_{\beta_0^2}}{\Omega^2}\beta_p
$$

where γ is the Lock number, $(\rho a c R^4/I_b)$, ω_{β_0} is the nonrotating flap frequency, β_p is the precone angle and ν_β is the rotating flap frequency in terms of rotational speed. The term $\omega_{\beta_0}^2$ is used to model a hingeless blade, or an articulated blade with a flap spring. For an articulated blade without a flap spring, this term is zero. In addition, if there is no hinge offset (teetering blade or gimballed blade) $\nu_\beta = 1$. The simplified flap equation in this case becomes

$$
\overset{**}{\beta} + \beta = \gamma\overline{M_\beta} \tag{1.32}
$$

Substitute $\overline{M_\beta}$ and β in the flap equation (1.21) and match the constant, $\cos\psi$, and $\sin\psi$ terms on both sides to obtain the solution as follows.

$$
\begin{aligned}
\nu_\beta^2\beta_0 &= \gamma\left[\frac{\theta_0}{8}(1+\mu^2)+\frac{\theta_{tw}}{10}(1+\frac{5}{6}\mu^2)+\frac{\mu}{6}\theta_{1s}-\frac{\lambda}{6}\right]+\frac{\omega_{\beta 0}^2}{\Omega^2}\beta_p \\
(v_\beta^2-1)\beta_{1c} &= \gamma\left[\frac{1}{8}(\theta_{1c}-\beta_{1s})\left(1+\frac{1}{2}\mu^2\right)-\frac{\mu}{6}\beta_0\right] \\
(v_\beta^2-1)\beta_{1s} &= \gamma\left[\frac{1}{8}(\theta_{1s}+\beta_{1c})\left(1-\frac{1}{2}\mu^2\right)+\frac{\mu}{3}\theta_0-\frac{\mu}{4}\lambda+\frac{\mu^2}{4}\theta_{1s}+\frac{\mu}{4}\theta_{tw}\right]
\end{aligned} \tag{1.33}
$$

The solution to (1.32) can be obtained by simply putting $\nu_\beta = 1$ in the above expressions.

$$
\begin{aligned}
\beta_0 &= \gamma\left[\frac{\theta_0}{8}(1+\mu^2)+\frac{\theta_{tw}}{10}(1+\frac{5}{6}\mu^2)-\frac{\mu}{6}\theta_{1s}-\frac{\lambda}{6}\right] \\
\beta_{1s}-\theta_{1c} &= \frac{-\frac{4}{3}\mu\beta_0}{1+\frac{1}{2}\mu^2} \\
\beta_{1c}+\theta_{1s} &= \frac{-\left(\frac{8}{3}\right)\mu\left[\theta_0-\frac{3}{4}\lambda+\frac{3}{4}\mu\theta_{1s}+\frac{3}{4}\theta_{tw}\right]}{1-\frac{1}{2}\mu^2}
\end{aligned} \tag{1.34}
$$

Recall that we studied the effect of cyclic pitch variation in hover. A sine input in cyclic produced a cosine output in flap, and vice-versa. This was when the rotor operated under resonance conditions where $\nu_\beta = 1$. The flap solution in forward flight for $\nu_\beta = 1$ is given above. Substitute $\mu = 0$ in the above expression to re-obtain the hover results.

Put $\mu = 0$ in the solution of equation (1.21).

$$\beta_{1s} - \theta_{1c} = 0$$

$$\beta_{1c} + \theta_{1s} = 0$$

This means for pitch variation

$$\theta = \theta_0 + \theta_{1c}\cos\psi + \theta_{1s}\sin\psi$$

The flap response will be

$$\beta = \beta_0 + \theta_{1c}\cos(\psi - 90^\circ) + \theta_{1s}\sin(\psi - 90^\circ)$$

Therefore, for articulated blades with zero hinge spring and zero hinge offset, the flap response lags pitch motion by 90° (resonance condition).

For a hingeless blades, or articulated blades with non-zero hinge springs, or articulated blades with non-zero hinge offsets, put $\mu = 0$ in the solution of (1.21).

$$\begin{aligned}
\beta_0 &= \frac{\gamma}{v_\beta^2}\left[\frac{\theta_0}{8} - \frac{\lambda}{6}\right] + \frac{\omega_{\beta 0}^2}{\Omega^2}\beta_p \\
\beta_{1s} &= \frac{\theta_{1c} + (v_\beta^2 - 1)\frac{8}{\gamma}\theta_{1s}}{1 + \left[(v_\beta^2 - 1)\frac{8}{\gamma}\right]^2} \\
\beta_{1c} &= \frac{-\theta_{1s} + (v_\beta^2 - 1)\frac{8}{\gamma}\theta_{1c}}{1 + \left[(v_\beta^2 - 1)\frac{8}{\gamma}\right]^2}
\end{aligned} \tag{1.35}$$

Thus θ_{1s} produces both β_{1s} and β_{1c}. Similarly θ_{1c} produces both β_{1s} and β_{1c}. This is an off-resonance condition where the forcing frequency is less than the natural frequency. Lateral flap deflection is now caused by longitudinal cyclic pitch θ_{1s}, in addition to lateral pitch θ_{1c}. Recall that the phase lag of flap response with respect to the pitch motion was shown earlier to be

$$\phi = 90^\circ - \tan^{-1}\frac{(\nu_\beta^2 - 1)}{\frac{8}{\gamma}}$$

1.4 Introduction to Loads

The distribution of aerodynamic and centrifugal forces along the span, and the structural dynamics of the blade in response to these forces create shear loads and bending loads at the blade root. For a zero hinge offset, the blade root is at the center of rotation. For a non-zero hinge offset, it is at a distance e outboard from the center of rotation. By 'loads' we mean 'reaction' forces generated by the net balance of all forces acting over the blade span. Let s_x, s_r, and s_z be the three shear loads, in-plane, radial, and vertical. Let n_f, n_t, and n_l be the bending loads, flap bending moment, torsion moment (positive for leading edge up), and chord bending moment (positive in lag direction). They occur at the blade root, rotate with the blade, and vary with the azimuth angle. Thus they are called the rotating root loads. Or simply root loads or root reactions.